Global Biogeochemical Cycles

RESEARCH ARTICLE
10.1029/2021GB007245

The Seasonality of Deuterium Excess in Non-Polar Precipitation

Zhengyu Xia[1,2], Jeffrey M. Welker[3,4], and Matthew J. Winnick[2]

[1]Key Laboratory of Geographical Processes and Ecological Security in Changbai Mountains, Ministry of Education, School of Geographical Sciences, Northeast Normal University, Changchun, China, [2]Department of Geosciences, University of Massachusetts Amherst, Amherst, MA, USA, [3]Department of Biological Sciences, University of Alaska Anchorage, Anchorage, AK, USA, [4]UArctic, Ecology and Genetics Research Unit, University of Oulu, Oulu, Finland

Key Points:

- Deuterium excess in precipitation is affected by multiple processes in the water cycle and an interpretative framework is needed
- Oceanic evaporation and raindrop re-evaporation effects dominate deuterium excess seasonality in mid-latitudes and low-latitudes, respectively
- Seasonal shifts in moisture recycling weakly affect deuterium excess due to terrestrial water storage and evapotranspiration partitioning

Supporting Information:

Supporting Information may be found in the online version of this article.

Correspondence to:

Z. Xia,
zhyxia@hotmail.com

Citation:

Xia, Z., Welker, J. M., & Winnick, M. J. (2022). The seasonality of deuterium excess in non-polar precipitation. *Global Biogeochemical Cycles*, *36*, e2021GB007245. https://doi.org/10.1029/2021GB007245

Received 7 NOV 2021
Accepted 3 OCT 2022

Abstract The deuterium excess (d-excess) of precipitation varies seasonally at sites across the globe, an observation that has often been linked to seasonal changes in oceanic evaporation conditions, continental moisture recycling, and subcloud raindrop re-evaporation. However, there have been very few studies to quantify and evaluate the relative importance of these processes. Here, we revisit the mechanisms of precipitation d-excess seasonality in low-latitudes and mid-latitudes through a new analysis of precipitation isotope databases along with climate reanalysis products and moisture tracking models. In low-latitudes, the raindrop re-evaporation effect, indicated by local relative humidity, exerts a strong and prevalent control on observed d-excess seasonality and overprints the effect of oceanic evaporation conditions. In mid-latitudes, the effect of oceanic evaporation conditions becomes stronger and seems dominant in the observed d-excess seasonality. However, the ultimate d-excess signals are produced after complex modulations by several reinforcing or competing processes, including prior distillations, moisture recycling, supersaturation in snow formation, and raindrop re-evaporation. Among these processes, substantial increases in the proportion of recycled moisture during the warm and dry season do not produce higher precipitation d-excess in mid-latitude continental interiors. We develop a simple seasonal water storage model to show that contributions of previously evaporated residual water storage and higher transpiration fractions may lead to relatively low d-excess in evapotranspiration fluxes during periods of enhanced continental moisture recycling. This study underscores the ubiquitous nonconservative behavior in d-excess throughout the water cycle, as opposed to using d-excess as a simple tracer for remote conditions at oceanic moisture sources.

1. Introduction

The isotopic composition of precipitation (defined as $\delta = (R_s/R_{std} - 1) \times 1{,}000‰$ where R_s and R_{std} are the molar ratio of $^{18}O/^{16}O$ or $^{2}H/^{1}H$ in the sample and Vienna Standard Mean Ocean Water standard, respectively) varies temporally and spatially in response to multiple scales of climate variations and land-atmosphere interactions due to isotopic fractionations in the water cycle (Dansgaard, 1964; Gat, 1996). Globally, isotopic variations of precipitation have been extensively documented by a large volume of observational data through the Global Network of Isotopes in Precipitation (GNIP) program (IAEA/WMO, 2021) and other national networks (Birks & Gibson, 2009; Wang et al., 2022; Welker, 2012). These data have been characterized for their empirical relationships with climate parameters (Bowen, 2008; Rozanski et al., 1993), spatial gradients (Liu et al., 2010; Salati et al., 1979), and long-term trends (Putman et al., 2021; Rozanski et al., 1992), with process-based models developed to explain the mechanisms of observed isotopic variations in space and time (Aggarwal et al., 2012; Bailey et al., 2018; Dansgaard, 1964; Hendricks et al., 2000; Konecky et al., 2019; Winnick et al., 2014). These seminal works support the use of water isotope measurements to investigate a range of (paleo-) climatological, hydrological, ecological, and biogeochemical problems (Bowen, 2010; Bowen et al., 2019). Still, many studies have only explored the isotopic variations of water through the single isotope system ($\delta^{18}O$ or $\delta^{2}H$ only).

The second-order isotopic parameter of precipitation, deuterium excess (defined as d-excess = $\delta^{2}H - 8 \times \delta^{18}O$), has also been frequently examined in isotope hydrology and climatology literature. Because of the difference in diffusivity of ^{18}O-containing or ^{2}H-containing water molecules, this dual isotope metric was conceived to track the component of kinetic fractionation that occurs with water phase changes in the hydrological cycle (Dansgaard, 1964), with a global average value of 10‰ that defines the Global Meteoric Water Line ($\delta^{2}H = 8 \times \delta^{18}O + 10$) (Craig, 1961). Analyses of "simple isotope models" based on the single-source Rayleigh

distillation model conclude that precipitation d-excess is highly sensitive to evaporative conditions at the oceanic moisture source where initial water vapor is formed, specifically by parameters including sea surface temperature (SST) and relative humidity (RH) above the ocean (Johnsen et al., 1989; Merlivat & Jouzel, 1979; Pfahl & Sodemann, 2014). As such, the d-excess has been primarily used as a proxy in Antarctic and Greenland ice core studies to reconstruct past changes in moisture source regions and conditions (Jouzel et al., 1982; Landais et al., 2021; Markle et al., 2017; Masson-Delmotte et al., 2005; Stenni et al., 2001; Vimeux et al., 1999). However, for precipitation over low-latitude and mid-latitude terrestrial environments, it is well known that the d-excess signal of ocean-derived water vapor is altered by other processes that involve kinetic fractionations (Froehlich et al., 2002), such as continental moisture recycling (Aemisegger et al., 2014; Froehlich et al., 2008; Gat & Matsui, 1991; Gat et al., 1994; Kong et al., 2013), snow formation where vapor deposition occurs in an environment that is supersaturated with respect to ice (Ciais & Jouzel, 1994; Dütsch et al., 2019; Jouzel & Merlivat, 1984), and local raindrop re-evaporation and equilibration (Graf et al., 2019; Landais et al., 2010; Liebminger et al., 2006; Stewart, 1975; Wang et al., 2016b).

GNIP monitoring stations worldwide show that precipitation d-excess has seasonal variations (Araguás-Araguás et al., 1998; Feng et al., 2009; Froehlich et al., 2002). This feature provides an opportunity to examine the process-based mechanisms of precipitation d-excess variability, and more broadly, the seasonal dynamics of the continental water cycle. One major recognized pattern is that precipitation d-excess values are lowest in summer and highest in winter in many mid-latitude stations (Feng et al., 2009; Gat, 1996; Rozanski et al., 1993). A simple interpretation has been given (Rozanski et al., 1993): the lower summer d-excess is caused by the lower RH over continents that facilitates subcloud raindrop re-evaporation, while the higher winter d-excess is caused by the lower RH over oceans (i.e., higher vapor pressure deficit) and reflects increased kinetic effects during oceanic evaporation. The same seasonal pattern in d-excess, but with a very large amplitude (up to 20‰), was found in the southern Tibetan Plateau and attributed to the shift in moisture source and transport between the Indian summer monsoon and winter westerlies (Tian et al., 2007). It was also found in Tianshan of arid central Asia where westerlies dominate year round (Tian et al., 2007) and was there interpreted to reflect the raindrop re-evaporation effect that is strong in hot and dry summer and weak in other seasons (Pang et al., 2011). By contrast, some stations in the north of the European Alps have the highest d-excess in summer and autumn, which has been linked to the recycling of evaporated moisture over continents (Froehlich et al., 2008). In the tropics, a station within the Amazon rainforest (São Gabriel da Cachoeira) contains two semiannual cycles of d-excess and has been interpreted to reflect the shift in oceanic moisture source regions driven by the migration of the Intertropical Convergence Zone (ITCZ; Feng et al., 2009), although precipitation across Amazon itself is supplied by a considerable fraction of recycled moisture (Ampuero et al., 2020; Eltahir & Bras, 1994; Gat & Matsui, 1991).

From the several examples above, it is evident that the seasonal pattern in d-excess at a site is often interpreted by invoking one specific mechanism; however, there has been little work to validate such interpretations or to holistically evaluate the relative importance of each process that all can affect d-excess, both locally and at broader regional scales. Moreover, the isotope-enabled General Circulation Models (GCMs) have limited skills in representing the d-excess as shown, for instance, in their biases in representing Local Meteoric Water Lines compared to actual observations (Putman et al., 2019; Steen-Larsen et al., 2017). This limitation may be improved by the recent progress in coupling GCMs with land surface models that better represent the d-excess of evapotranspiration (ET) fluxes (Haese et al., 2013; Henderson-Sellers et al., 2006; Jouzel et al., 2013; Risi et al., 2016; Wong et al., 2017). Currently, the d-excess output from isotope-enabled GCMs is often used to constrain model physics or to tune model parameters (Dee et al., 2015; Dütsch et al., 2019; Risi et al., 2010), rather than to make inferences about moisture source conditions (Jouzel et al., 2013; Lewis et al., 2013). Overall, the knowledge gap of fundamental controls of precipitation d-excess limits the capacity to leverage the information of small, but existing, kinetic fractionation in the hydrological cycle for investigating scientific problems that are difficult to address with the single isotope system ($\delta^{18}O$ or $\delta^{2}H$), such as tracking the influence of sea ice retreat on atmospheric moisture budget (Klein & Welker, 2016; Klein et al., 2016; Kopec et al., 2016), measuring or partitioning ET fluxes (Froehlich et al., 2008; Gat & Matsui, 1991; Jasechko et al., 2013; Wang et al., 2016a), and distinguishing the contribution of snow, ice, and rain in river discharge (Lisi et al., 2015; Penna et al., 2014; Welp et al., 2005). In addition, recent advances in high-precision triple oxygen isotope measurements add a new interest in the excess term of ^{17}O, $\Delta'^{17}O$, which is defined for the same purpose as d-excess, as a tracer in hydrological and paleoclimate studies (Angert et al., 2004; Aron et al., 2021; Luz & Barkan, 2010; Sha et al., 2020). As both d-excess and $\Delta'^{17}O$ should follow essentially the same geochemical principles, there is a need to first understand how the sum

of a diversity of processes within the hydrological cycle is expressed in the variations of continental precipitation d-excess.

In this contribution, we present a new analysis to revisit the mechanisms of precipitation d-excess seasonality in low-latitudes and mid-latitudes. Our approach comprises large-scale statistical analyses of precipitation d-excess and climate reanalysis data as well as more detailed examinations of a subset of well-characterized, representative sites. Specifically, we apply moisture tracking models to quantify the role of oceanic source evaporation and continental moisture recycling. In Section 2, we describe the source and treatment of all data, moisture tracking models, and conducted analyses. In Section 3, we discuss the bias in precipitation d-excess data and justify using condensation-corrected vapor d-excess for our analysis. In Section 4, we summarize the spatial patterns of correlations between d-excess and major driving variables (oceanic evaporation conditions, moisture recycling, and raindrop re-evaporation), which elucidate the primary large-scale controls. In Section 5, we seek to disentangle the respective role of each process in producing the observed d-excess seasonality at representative sites. In Section 6, we investigate an emergent observation that the large seasonal shift in ET appears to be a relatively unimportant control on d-excess seasonality. We develop a simple water storage model to show how the d-excess of ET fluxes responds to seasonal changes in land surface ecohydrology. Finally, in Section 7, we summarize the major findings and impacts of this contribution.

2. Data and Methods

2.1. Isotope Data

We compiled GNIP monthly precipitation isotope data and included all stations between 60°N and 60°S (IAEA/WMO, 2021). To increase the coverage for the contiguous US, we additionally included the US Network for Isotopes in Precipitation (USNIP) weekly precipitation isotope data from 1989 to 2001 (Data Set S1; Welker, 2000, 2012). To remove potentially erroneous data recordings, we screened both databases by excluding individual observations with $\delta^{18}O > 5‰$, d-excess $< -15‰$, or d-excess $> 30‰$, which are likely results of typographical errors or mishandling of samples.

We calculated 12 monthly arithmetic mean precipitation $\delta^{18}O$ and d-excess values and their uncertainties using the standard error of the mean (SEM, SEM = SD/$\sqrt{n}$ where SD is the standard deviation and n is the number of observations) for each station if that month has at least 3 (GNIP monthly) or 6 (USNIP weekly) d-excess observations, and if not, we treated that month as a data gap. Based on the derived monthly d-excess statistics, we further removed stations with >6 monthly data gaps. We used arithmetic means rather than amount-weighted means as we aim to represent an "average year" (Bowen et al., 2005), with no bias toward heavy precipitation periods. We used SEM rather than SD as we are interested in the uncertainty of monthly mean d-excess that together define the d-excess seasonality rather than how variable it is for the respective month. We also calculated seasonal arithmetic mean $\delta^{18}O$ and d-excess values likewise for December–February (DJF), March–May (MAM), June–August (JJA), September–November (SON), with at least 6 (GNIP) or 12 (USNIP) monthly observations. The final data set contains 524 stations (459 GNIP and 65 USNIP stations), although a few GNIP stations are in very close locations but identified by different station codes.

The above monthly d-excess statistics are derived from raw precipitation d-excess data ("RP d-excess"). However, the d-excess is not conserved when vapor shifts to liquid or ice, a fact that has been described previously (Gat et al., 1994; Guan et al., 2013; Pfahl & Wernli, 2008). The d-excess may either increase or decrease in condensate relative to water vapor and the magnitude of changes could be as high as >10‰ (Graf et al., 2019). To correct this local condensation effect on RP d-excess, we converted all precipitation isotope data (δ_p) into their corresponding vapor values (δ_{cv}) using fractionation factors and then derived the second set of monthly d-excess statistics ("CV d-excess") following the same data processing procedure

$$\delta_{cv} = \frac{(\delta_p + 1,000)}{\alpha} - 1,000 \quad (1)$$

where α is the fractionation factor based on condensation temperature (T_d in degree Celsius). For $T_d \geq 0$ °C, the condensate is assumed purely liquid and α is the liquid-vapor equilibrium fractionation (α_{eq}^{l-v}) as

$$\alpha = \alpha_{eq}^{l-v} = \exp\left[\frac{1,137}{(T_d + 273.15)^2} - \frac{0.4156}{T_d + 273.15} - 0.00207\right] \text{ for } \delta^{18}O \text{ (Majoube, 1971b)} \quad (2)$$

and

$$\alpha = \alpha_{eq}^{l-v} = \exp\left[\frac{24,844}{(T_d + 273.15)^2} - \frac{76.248}{T_d + 273.15} + 0.05261\right] \text{ for } \delta^2\text{H (Majoube, 1971b)} \quad (3)$$

For $T_d \leq -15$ °C, the condensate is assumed purely ice and α combines the ice-vapor equilibrium fractionation (α_{eq}^{i-v}) and the kinetic fractionation (α_k^{i-v}) that occurs in vapor deposition due to supersaturation over ice as

$$\alpha = \alpha_{eq}^{i-v}\alpha_k^{i-v} \quad (4)$$

$$\alpha_{eq}^{i-v} = \exp\left[\frac{11.839}{T_d + 273.15} - 0.028224\right] \text{ for } \delta^{18}\text{O (Majoube, 1971a)} \quad (5)$$

$$\alpha_{eq}^{i-v} = \exp\left[\frac{16,289}{(T_d + 273.15)^2} - 0.0945\right] \text{ for } \delta^2\text{H (Merlivat \& Nief, 1967)} \quad (6)$$

and

$$\alpha_k^{i-v} = \frac{S_i}{\alpha_{eq}^{i-v}(D/D')(S_i - 1) + 1} \text{ (Jouzel \& Merlivat, 1984)} \quad (7)$$

where D/D' is the ratio of diffusivity between light and heavy isotope species and is 1.0285 for $^{16}O/^{18}O$ and 1.0251 for $^1H/^2H$ (Merlivat, 1978). S_i is the supersaturation ratio over ice assumed to vary linearly with T_d following the form $S_i = 1 - \lambda T_d$ (Jouzel & Merlivat, 1984), where λ is a sensitivity parameter tuned to yield a reasonable d-excess output in both isotope-enabled GCMs (e.g., Risi et al., 2010; Schmidt et al., 2005; Werner et al., 2011) and "simple isotope models" (e.g., Johnsen et al., 1989; Jouzel & Merlivat, 1984; Petit et al., 1991). These ice-vapor fractionations have been recently validated in laboratory experiments (Lamb et al., 2017). We set $\lambda = 0.004$ in this study, consistent with some GCMs (Lee et al., 2007; Risi et al., 2010; Schmidt et al., 2005). For -15 °C $< T_d < 0$ °C, α is linearly interpolated between α end-members when $T_d = -15$ °C and 0 °C to approximate mixed-phase cloud conditions where supercooled liquid and solid condensate coexist (Ciais & Jouzel, 1994; Yoshimura et al., 2008). This condensation-corrected, second set of monthly d-excess statistics is the main data set for the following analysis and discussion as justified in Section 3.

2.2. Reanalysis Data

We used the European Centre for Medium-Range Weather Forecasts (ECMWF) ERA5 reanalysis (0.25° × 0.25°) (C3S, 2021; Hersbach et al., 2020) monthly data fields spanning 1981–2010 for several purposes. First, the 12 monthly means of 2-m dew temperature were used to calculate CV d-excess for each station described in Section 2.1. The uncertainty of 2-m dew temperature was not considered when CV d-excess was calculated. Second, because our previous work showed that surface RH strongly controls the magnitude of change in d-excess by local raindrop re-evaporation (Xia & Winnick, 2021), we calculated 12 monthly means and SEMs of surface RH (h_s) for each station from the Clausius-Clapeyron relation, using 2-m air temperature (T) and dew temperature (T_d) in degree Celsius as

$$h_s = \exp\left[\frac{17.67T_d}{T_d + 243.5} - \frac{17.67T}{T + 243.5}\right] \times 100\% \text{ (Bolton, 1980)} \quad (8)$$

We used local surface RH as a metric to represent the effect of raindrop re-evaporation. Third, we used reanalysis data to calculate oceanic RH with respect to SST to model the oceanic vapor d-excess described in more details in Section 2.4. For this purpose, in addition to 2-m dew temperature, necessary data fields include SST, latent heat flux, sea-ice cover, vertically integrated moisture divergence, and lake cover. Fourth, we used 12 monthly means of precipitation and ET fluxes (evaporation field in ERA5 reanalysis) to investigate the seasonal changes in surface water balance.

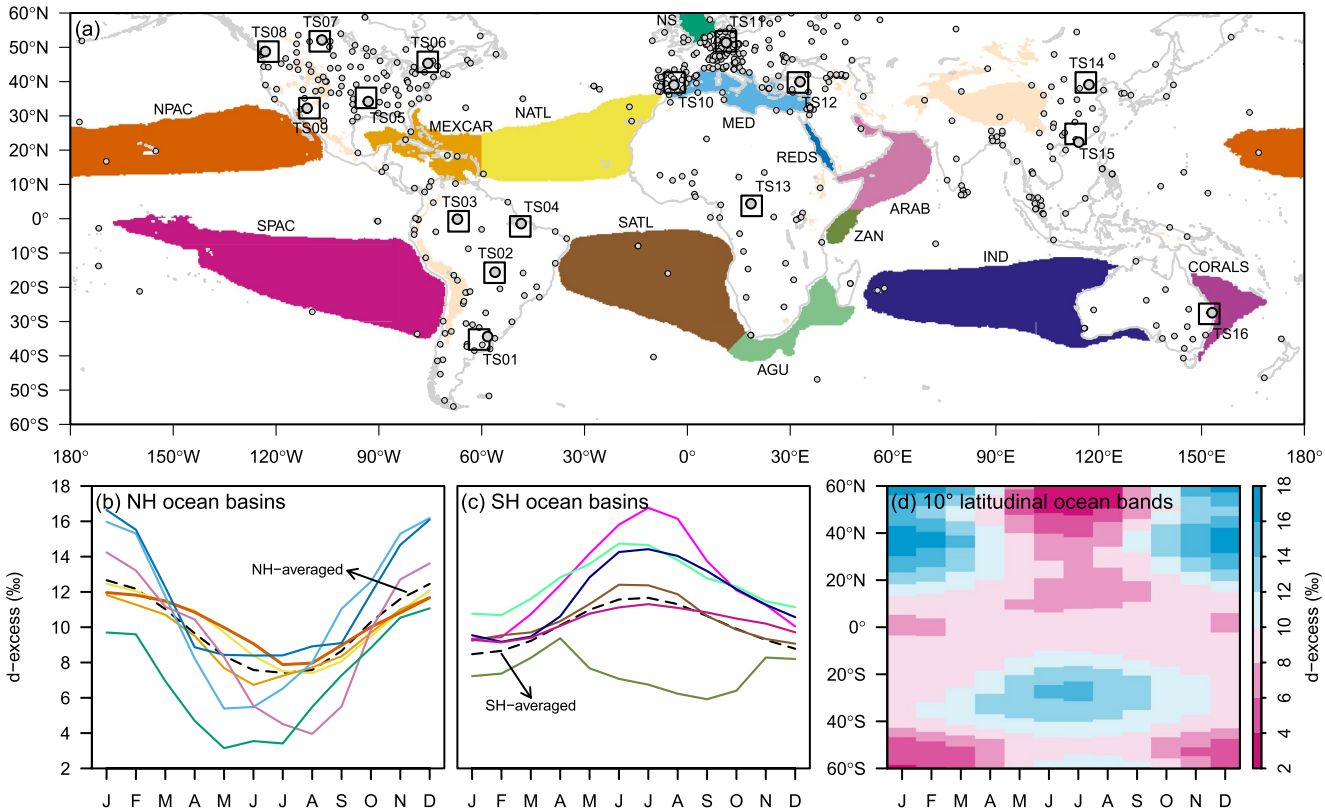

Figure 1. (a) The map showing the locations of analyzed GNIP/USNIP stations (gray dots), 12 oceanic moisture sources by Gimeno et al. (2010) plus the North Sea (colored areas), and 16 target sink (TS) areas (black boxes) for the WAM-2layers moisture source diagnostics. The larger gray dots are those representative sites listed in Table 1. The peach color on continents is areas with elevation >2,000 m (also for Figures 5 and 6). The 12 monthly means of oceanic vapor d-excess for Gimeno et al. (2010) ocean basins, with the same color code as in (a), as well as the hemisphere average values computed from the linear model, are shown in (b) for the Northern Hemisphere and (c) for the Southern Hemisphere. Also shown in (d) are the 12 monthly means of oceanic vapor d-excess from 10° latitudinal bands of oceans where the *y*-axis is the midpoint latitude of each band. The abbreviations for those ocean basins in (a) are: NPAC, North Pacific; MEXCAR, Mexico Caribbean; NATL, North Atlantic; NS, North Sea; MED, Mediterranean Sea; REDS, Red Sea; ARAB, Arabian Sea; SPAC, South Pacific; SATL, South Atlantic; AGU, Agulhas Current; ZAN, Zanzibar Current; IND, Indian Ocean; CORALS, Coral Sea (Gimeno et al., 2010).

2.3. Moisture Tracking Models

Moisture recycling with kinetic fractionations is often invoked as a mechanism for increasing precipitation d-excess in continental interiors (Ampuero et al., 2020; Froehlich et al., 2008; Gat & Matsui, 1991; Gat et al., 1994; Taupin et al., 2000; Xia & Winnick, 2021). To represent the effect of moisture recycling for each station, we run the Eulerian Water Accounting Model (WAM-2layers) version 2.4.08 (van der Ent, 2016) in forward tracking mode to derive 12 monthly means and SEMs of gridded continental precipitation recycling ratio (CPRR) spanning 1981–2010. Physically, the CPRR means the fraction of precipitation at a given location that originates from terrestrial moisture sources (including evaporation from lakes), in contrast to that of oceanic sources (van der Ent et al., 2014). For convenience, the model was forced by the lower resolution ERA-Interim reanalysis (1.5° × 1.5°; Dee et al., 2011), between 79.5°N and 79.5°S, which is the default option of the WAM-2layers.

To diagnose the moisture source regions that are used to calculate the oceanic source vapor d-excess, we again run the WAM-2layers, but in backward tracking mode, to reconstruct the gridded monthly tracked evaporation flux over oceans (E_o) that precipitates out at a given sink area spanning 1981–2010. This was accomplished by replacing the land-sea mask with one that only covers the sink grids, which correspond to an area of interest (Cluett et al., 2021; van der Ent, 2016). The same approach has been applied to reconstruct the "precipitation-shed" for an area of interest to quantify the spatial dependence of local precipitation on upwind evaporation over lands and oceans (Keys et al., 2012). Due to the high computational cost of these analyses, we selected only 16 representative GNIP/USNIP stations for moisture source diagnostics and the target sinks were set as 6° × 6° areas that contain each site (Figure 1a and Table 1). These GNIP/USNIP stations were chosen for their global coverage

Table 1
Target Sink (TS) Areas for the WAM-2layers Moisture Source Diagnostics With Their Representative GNIP/USNIP Stations Shown in Figure 1

ID	Area	Station and code
TS01	Pampas Argentina	Buenos Aires-Cd. Universitaria (8757601)
TS02	Central-West Brazil	Cuiabá (8336101)
TS03	Amazon	São Gabriel da Cachoeira (8210600)
TS04	Northern Brazil	Belem (8219100)
TS05	Central US	Caddo Valley (AR03)[a]
TS06	Eastern Canada	Ottawa (7162800)
TS07	Western Canada	Saskatoon (7186601)
TS08	Pacific Northwest	Saturna (7191400)
TS09	Southwestern US	Tucson (7227401)
TS10	Spain	Ciudad Real (834801)
TS11	Germany	Artern (1046000)
TS12	Turkey	Ankara (1713000)
TS13	Equatorial Africa	Bangui-Université (6465002)
TS14	Northern China	Tianjin (5452700)
TS15	Southern China	Hong Kong (4500400)
TS16	Eastern Australia	Brisbane (9457600)

[a]USNIP station.

in geography and different climates. They exhibit well-characterized d-excess seasonality with small errors (measured by SEM) and are not too short in duration (>10 years except for two sites).

2.4. Oceanic Vapor d-Excess

To quantify the oceanic source vapor d-excess for each representative site of WAM-2layers moisture source diagnostics, we applied a linear model that links boundary layer vapor d-excess above oceans to oceanic RH with respect to SST (h_{SST}) as

$$\text{d}-\text{excess}\,(‰) = 48.2 - 0.54 \times h_{SST}\,(\%)\,(\text{Pfahl \& Sodemann, 2014}) \quad (9)$$

This linear regression model is constructed based on existing observations and is accurate to close the hemisphere d-excess budget between sources and sinks (Pfahl & Sodemann, 2014). It does not rely on the "closure assumption" (Jouzel & Koster, 1996; Merlivat & Jouzel, 1979), specific boundary layer regime (Pfahl & Wernli, 2009), or GCM physics (Risi et al., 2013; Steen-Larsen et al., 2017), to derive the d-excess of oceanic vapor. Other vapor observations support the accuracy of this simple regression model (Benetti et al., 2014; Steen-Larsen et al., 2014). We derived a product of gridded monthly h_{SST} with Equation 8 by replacing 2-m air temperature with SST, between 79.5°N and 79.5°S consistent with the WAM-2layers. Any monthly $h_{SST} > 110\%$, the upper bound of the calibration data set in Pfahl and Sodemann (2014), was set to 110%. For diagnosed moisture source regions, we calculated monthly spatially averaged h_{SST}, by averaging h_{SST} from all ocean grids (0.25° × 0.25°, not including sea ice and lakes) weighted by gridded E_o (1.5° × 1.5°). We then derived 12 monthly means of oceanic vapor d-excess spanning 1981–2010 following the linear regression model.

Moreover, we similarly calculated a variety of other reference oceanic vapor d-excess using ERA5 reanalysis for comparison and discussion. Specifically, we calculated 12 monthly means of oceanic vapor d-excess spanning 1981–2010, averaged by weighting grid box area and latent heat flux, over: (a) the Northern and Southern Hemispheres as in Pfahl and Sodemann (2014), but within 79.5°N and 79.5°S; (b) the 12 oceanic moisture sources defined by Gimeno et al. (2010) based on the threshold of 750 mm yr^{-1} mean annual vertically integrated moisture flux divergence, plus the North Sea (Figure 1a); (c) all 10° latitudinal bands from 60°N to 60°S; and (d) the nearest 1,000 ocean grids (0.25° × 0.25°) for each analyzed station. The (c) and (d) are useful for site-level correlation analysis described in Section 2.5. Note that Pfahl and Sodemann (2014) used h_{SST} and latent heat flux data at 6-hr temporal resolution to calculate oceanic vapor d-excess, but they concluded that monthly h_{SST} and latent heat flux data, which were used in this study, did not impact the results.

For each derived monthly mean of oceanic vapor d-excess, its uncertainty was estimated using a Monte Carlo (MC) approach in which we resampled 10^4 d-excess values considering both the uncertainty of monthly spatially averaged h_{SST} (interannual variability from 1981 to 2010) and the uncertainty of the linear regression model (see Figure 1a of Pfahl and Sodemann (2014)). The SEM of oceanic vapor d-excess is <1‰ and is dominated by the uncertainty of the linear regression model, while the contribution of monthly spatially averaged h_{SST} is very small because it is a weighted average value over numerous ocean grids. However, we are unable to evaluate and incorporate the uncertainty related to reanalysis products.

2.5. Statistical Analysis

We developed a statistical MC correlation approach to analyze the seasonal control of oceanic vapor d-excess, local CPRR, and local RH on CV d-excess in each station. We hypothesize that the higher oceanic vapor d-excess, higher local CPRR, and higher local RH, which collectively are assumed to represent the primary forcing mechanisms, should each result in the higher CV d-excess as a response variable on seasonal time scales. For each station, Pearson's correlation was tested 10^4 times between the pair of a driving variable and CV d-excess, each

time we created a suite of randomly resampled 12 monthly values for both variables following Gaussian distributions based on their monthly means and SEMs. To represent the oceanic vapor d-excess, the 10° latitudinal band and nearest ocean vapor d-excess that are available for all stations were used for correlation analysis. We removed months with $T_d < -5$ °C when testing the MC correlation between local RH and CV d-excess, as the raindrop re-evaporation effect should not diminish further within the range of subfreezing temperature (Liebminger et al., 2006). If over 50% of MC correlations had Pearson's $R > 0$ with $p < 0.05$ between a certain driving variable and CV d-excess, we considered that they have a significantly positive MC correlation that is not prone to errors.

As this MC correlation approach incorporates the uncertainty and variability in reanalysis variables and d-excess observations, we view it as a more conservative measure of correlation than correlations between 12 monthly means of two variables. It is possible to set a more strict correlation threshold. For example, some statistical analyses of geochemical data required >95% of created MC correlations to be statistically significant (Li et al., 2016). However, such a strict threshold would dramatically reduce the number of stations with significant MC correlations in our data set, because the number of data points for the correlation pair is at most only 12 while the *p*-value is often high with such a small sample size (under the same correlation *R*-value).

3. The Condensation Effect on d-Excess

In Figures 2 and 3, we show both the RP and CV d-excess of 16 representative GNIP/USNIP stations that we have run the WAM-2layers moisture source diagnostics. For example, it is clear that the CV d-excess may show different seasonal patterns from the RP d-excess due to the shift in d-excess in condensation. In Caddo Valley (Arkansas, US) and Hong Kong, the CV d-excess reaches the highest values while the RP d-excess reaches the lowest values in JJA, leading to opposite seasonal patterns (Figures 2e and 3g). In Buenos Aires, the CV d-excess reaches the highest values in MAM and the lowest values in JJA, but RP d-excess reaches the highest values in September and the lowest values in DJF (Figure 2a). Although the slight offset between CV and RP d-excess itself is not surprising (Gat et al., 1994; Graf et al., 2019; Guan et al., 2013; Pfahl & Wernli, 2008), it is a new finding that different seasonal patterns in d-excess may emerge after correcting this local condensation effect.

Theoretically, the attendant offset between RP and CV d-excess is controlled not only by T_d and its associated fractionation factors, but also by the absolute values of RP $\delta^{18}O$ and d-excess (or, more accurately, δ^2H). In Figure 4, using Equations 1–7, we quantify the predicted range and direction of this offset and their relationships with T_d and RP $\delta^{18}O$ when RP d-excess is prescribed at 10‰. The predicted offsets, CV d-excess minus RP d-excess, are shown as contour lines. We note that using different RP d-excess values from 0‰ to 20‰ only slightly shift those plotted contour lines (not shown), thus the effect of RP d-excess is minimal. Therefore, we add to the plot the distribution of all monthly mean RP $\delta^{18}O$ and T_d in our GNIP/USNIP data sets (regardless of their RP d-excess).

For $T_d > 0$ °C, the shape of contour lines indicates that lower T_d and higher RP $\delta^{18}O$ result in more negative d-excess offsets (further lower CV d-excess than RP d-excess). Most GNIP/USNIP observations plot within the space of negative d-excess offsets when $T_d < 20$ °C, while positive d-excess offsets are common when $T_d > 20$ °C. The range of these offsets is <±3‰ for most observations. We highlight in Figure 4, the 12 monthly means of T_d and RP $\delta^{18}O$ from Caddo Valley, Hong Kong, and Buenos Aires to illustrate their impacts on their own d-excess offsets. In Caddo Valley, large seasonal changes in T_d cause positive d-excess offsets in summer and negative d-excess offsets in winter, which in turn lead to the opposite CV and RP d-excess seasonality. In Hong Kong, the opposite seasonality in CV and RP d-excess is the result of seasonal changes in both T_d and RP $\delta^{18}O$ that act together to cause positive d-excess offsets in summer monsoon season and negative d-excess offsets in winter. In Buenos Aires, seasonal changes in T_d and RP $\delta^{18}O$ follow a "circle trajectory" and lead to a more complex pattern in d-excess offsets. In MAM, the RP $\delta^{18}O$ reaches the lowest values (about −7‰), which results in slightly positive d-excess offsets and the highest CV d-excess. In JJA, the T_d reaches the lowest values (about 8 °C), which result in negative d-excess offsets and the lowest CV d-excess.

For $T_d < 0$ °C, the fractionation between vapor and precipitation is not purely equilibrium and the d-excess offset hinges on the parameterization of mixed-phase clouds and supersaturation conditions. Based on other parameterizations applied in isotope-enabled GCMs, we evaluate the sensitivity of this parameterization effect by plotting in Figure 4 the contour lines of zero when we set the tunable sensitivity parameter $\lambda = 0.003$ (Kurita et al., 2011; Yoshimura et al., 2008), $\lambda = 0.005$ (Tindall et al., 2009), or if we assume a wider temperature range

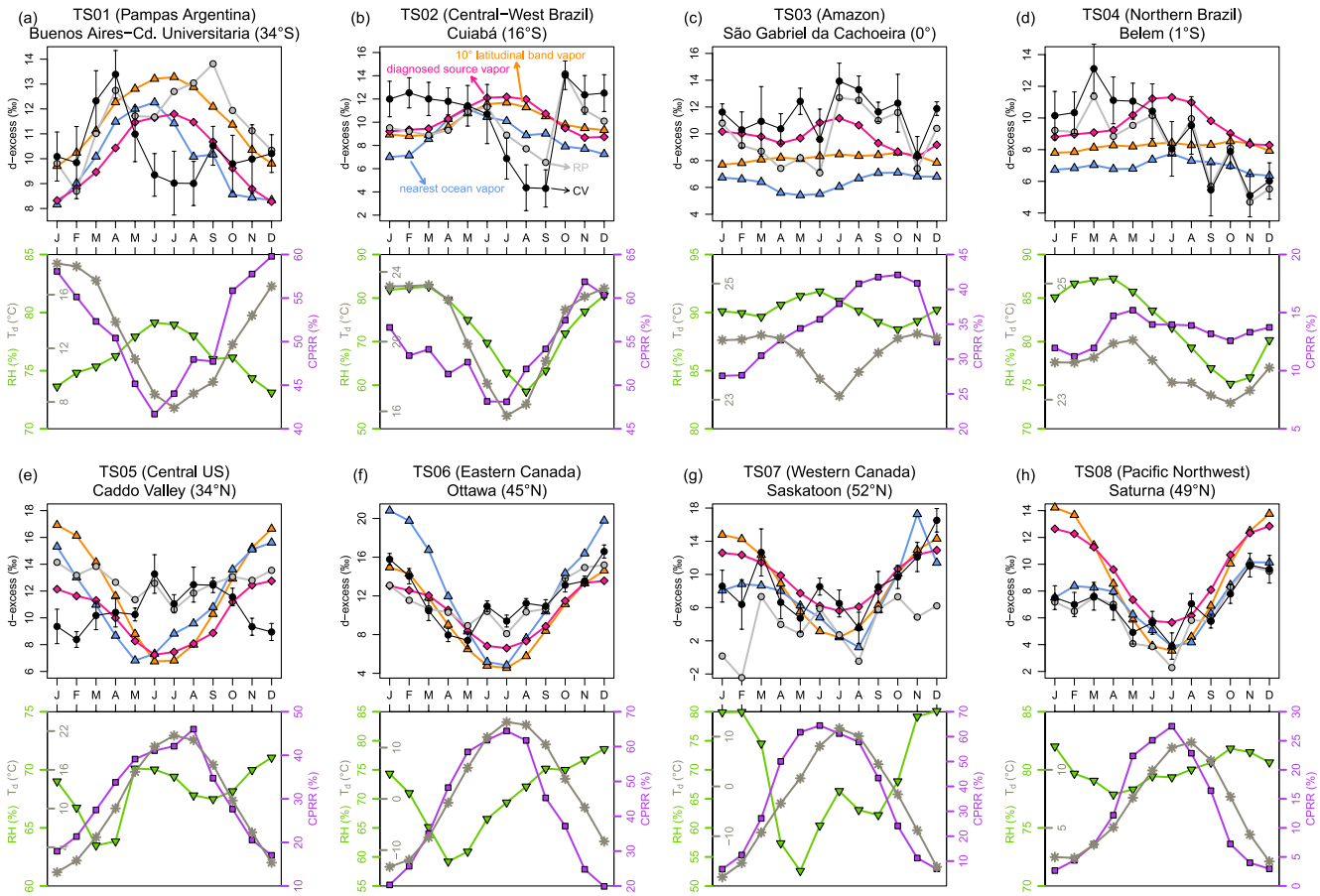

Figure 2. The 12 monthly means of diagnosed oceanic source vapor d-excess (pink diamonds) for the first 8 of 16 representative GNIP/USNIP stations are compared with their raw precipitation (RP; gray dots) and converted vapor (CV; black dots) d-excess data and the 10° latitudinal band (orange triangles) and nearest ocean (blue triangles) vapor d-excess. Also shown are the 12 monthly means of local T_d (gray asterisks), continental precipitation recycling ratio (CPRR; purple squares), and relative humidity (RH; green inverted triangles). The standard error of the means (SEMs) of CV d-excess are shown as error bars, which are relatively larger than the SEMs of other metrics. Note different *y*-axis scales for each subplot.

of mixed-phase cloud conditions down to −30 °C (Schmidt et al., 2005). Using these contour lines as a reference, it is found that up to ±6‰ deviation could occur by different parameterizations alone under very low T_d. These comparisons caution that large uncertainties exist in CV d-excess signals across subfreezing temperatures owing to the elusive supersaturation conditions.

The above analysis on the offset between RP and CV d-excess suggests that local condensation itself may affect or impair the seasonal pattern in d-excess observed in precipitation observations, but this isotopic effect in condensation carries little information about the large-scale dynamics. By correcting this isotopic effect, we are essentially acting to filter out the local condensation noises, which modify or even may overprint the effects of seasonal variability in upwind processes including oceanic moisture source regions and conditions as well as distillation and moisture recycling histories along transport pathways. While almost all literature does not make this correction and reaches their inferences based on RP d-excess data (e.g., Araguás-Araguás et al., 1998), we argue that the CV d-excess is more accurate to reflect the information about the large-scale dynamics, which after all are our primary interest in d-excess. This critical caveat justifies our following analysis and discussion only on CV d-excess data.

4. Spatial Patterns of Correlations Between d-Excess and Driving Variables

In Figure 5, we show the spatial distributions of GNIP/USNIP stations in which the CV d-excess has a significantly positive MC correlation with the 10° latitudinal band or nearest ocean vapor d-excess, local CPRR, and local RH. For comparison, we show in Figure S1 in Supporting Information S1 the results of correlation analysis

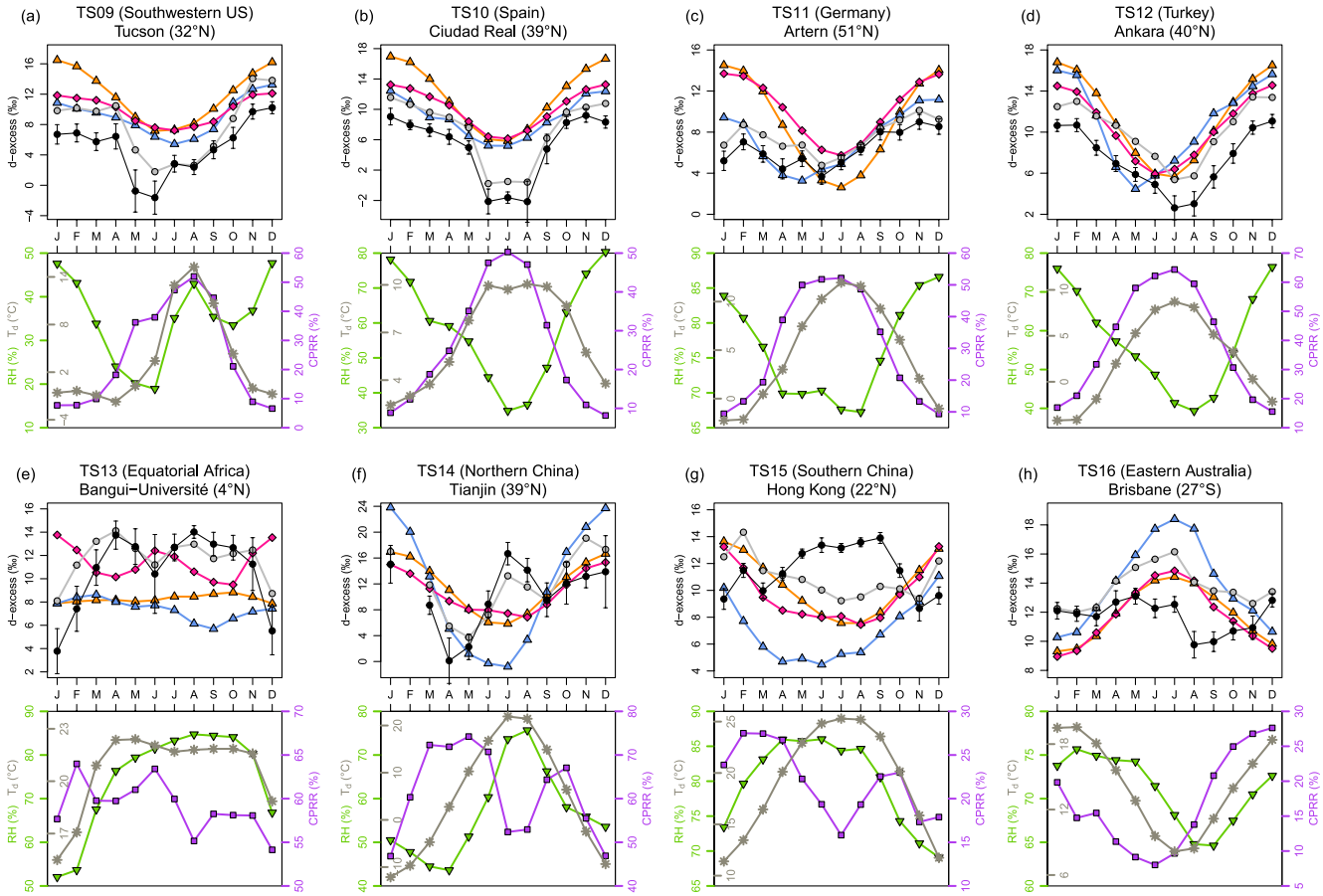

Figure 3. Same as Figure 2, but for the rest of the representative GNIP/USNIP stations.

using simple 12 monthly means of two variables. In these supplementary plots, more stations exhibit significantly positive correlations with those driving variables at $p < 0.05$, while our more conservative MC approach excluded those correlations that are not robust over errors.

To provide context for the spatial patterns of correlations between oceanic vapor and site CV d-excess, we first plot in Figures 1b and 1c the modeled oceanic vapor d-excess from the 12 oceanic moisture sources defined by Gimeno et al. (2010) plus the North Sea, and in Figure 1d the modeled oceanic vapor d-excess from 10° latitudinal bands. Overall, the oceanic vapor d-excess shares the same pattern of low summer and high winter values among different ocean basins, but the magnitude of seasonal variations is larger in higher latitudes. Still, the timing of the lowest d-excess in the Northern Hemisphere slightly differs among ocean basins. Specifically, Mexico Caribbean, North Sea, and Mediterranean ocean basins have the lowest vapor d-excess in May–June, at least 1 month earlier than the hemisphere average pattern, whereas North Atlantic and Arabian Sea ocean basins have the lowest vapor d-excess in August (Figure 1b). We also plot in Figure 6 the seasonal mean CV d-excess from GNIP/USNIP stations. These precipitation station data show comparable latitudinal and temporal patterns with oceanic vapor d-excess on seasonal time scales but with a few distinct regional anomalies. For example, there is a relatively high d-excess (>10‰) in inland South America across 0–30°S and a relatively low d-excess (<10‰) in western Europe in DJF, which contrast with the pattern of 10° latitudinal band vapor d-excess (Figure 6a). In addition, there is a relatively high d-excess (>10‰) in the eastern US and Southeast Asia in JJA as north as 40°N despite that only the latitude south to 10°S has such high oceanic vapor d-excess (Figure 6c). Furthermore, in Europe, the d-excess is much lower in MAM than in SON (Figures 6b and 6d).

Significantly positive MC correlations between oceanic vapor and site CV d-excess are mostly found in mid-latitude stations (Figure 5a), despite the large seasonality in CPRR (gray areas in Figure 5a). This pattern may reflect the fact that the amplitude of seasonal variations in oceanic vapor d-excess, or namely the strength

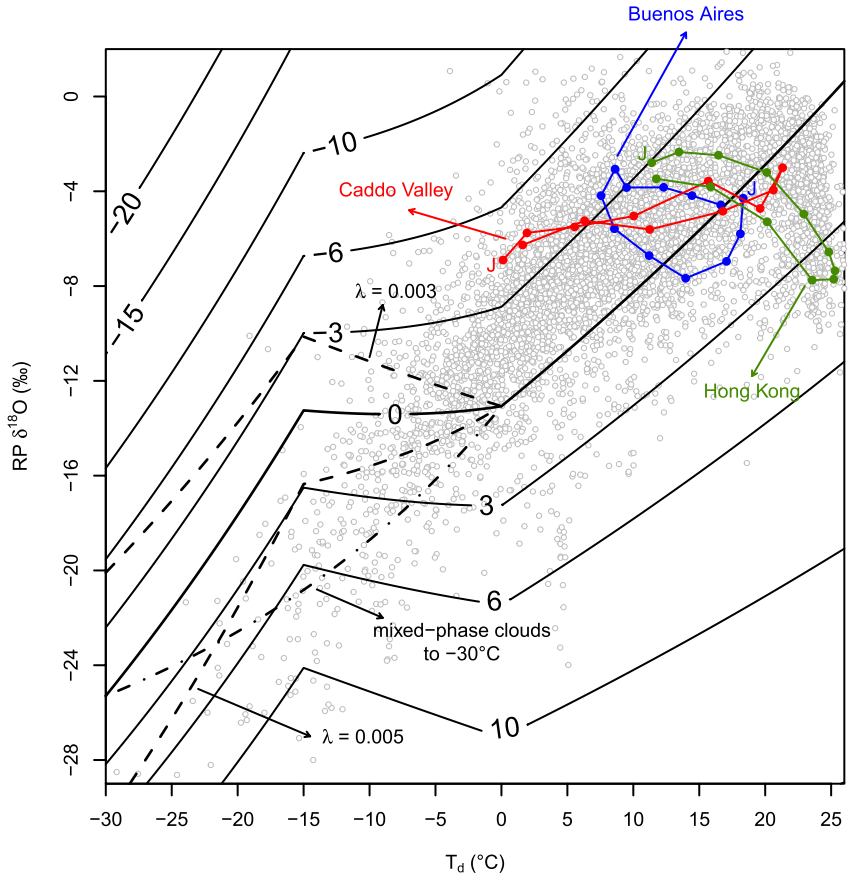

Figure 4. The predicted d-excess offsets, that is converted vapor (CV) d-excess minus raw precipitation (RP) d-excess, are shown in contour lines given a range of T_d and RP $\delta^{18}O$ with RP d-excess at 10‰. The zero contour line is thicker. The dashed lines are the results when we assume $\lambda = 0.003$ or $\lambda = 0.005$ and the dash-dotted line is the result when we assume the mixed-phase cloud conditions down to −30 °C. GNIP/USNIP monthly mean RP $\delta^{18}O$ observations and their ERA5 monthly mean T_d are plotted in gray dots. The 12 monthly means of RP $\delta^{18}O$ and T_d from Caddo Valley, Hong Kong, and Buenos Aires are highlighted in red, green, and blue dots and lines as a sequence and the label "J" indicates January.

of oceanic moisture source effect, is larger in mid-latitudes than in low-latitudes (Figure 1d). In isotope-based GCMs, it has been similarly found that there is a close link between latitudinal means of precipitation d-excess and oceanic evaporation conditions in mid-latitudes on seasonal time scales (Risi et al., 2013). In our correlation analysis, we distinguished two metrics of oceanic vapor evaporated from the 10° latitudinal band and the nearest ocean, respectively, to presumably represent remote and adjacent oceanic evaporation conditions. Among these correlations, it appears that the oceanic vapor across the 10° latitudinal band has a stronger control in North America and the oceanic vapor from the nearest ocean has a stronger control in Europe (Figure 5a). However, neither metric represents the oceanic vapor d-excess signal at the actual moisture source regions for each site. By contrast, a previous study has argued that oceanic evaporation at the latitude of subtropical highs is the primary moisture source and driver of d-excess variations for mid-latitude precipitation and has excluded oceanic evaporation from local oceans (Feng et al., 2009). While correlation patterns provide empirical evidence for the primacy of the oceanic moisture source effect in mid-latitudes, which has been well recognized in the literature (Feng et al., 2009; Froehlich et al., 2002; Gat, 1996; Rozanski et al., 1993), little information is known about the degree of phase coherency between oceanic vapor and site CV d-excess and the potential modifications by other processes. Therefore, moisture source diagnostics are required to gain quantitative insights into to what degree the oceanic source vapor d-excess is imprinted in the observations in precipitation.

Only a few stations such as in the southern US, Africa, and South American Andes have significantly positive MC correlations between local CPRR and site CV d-excess (Figure 5b). In mid-latitude North America and Eurasia, the CPRR shifts by >40% seasonally (gray areas in Figure 5b), peaking in summer (Figure 7). With

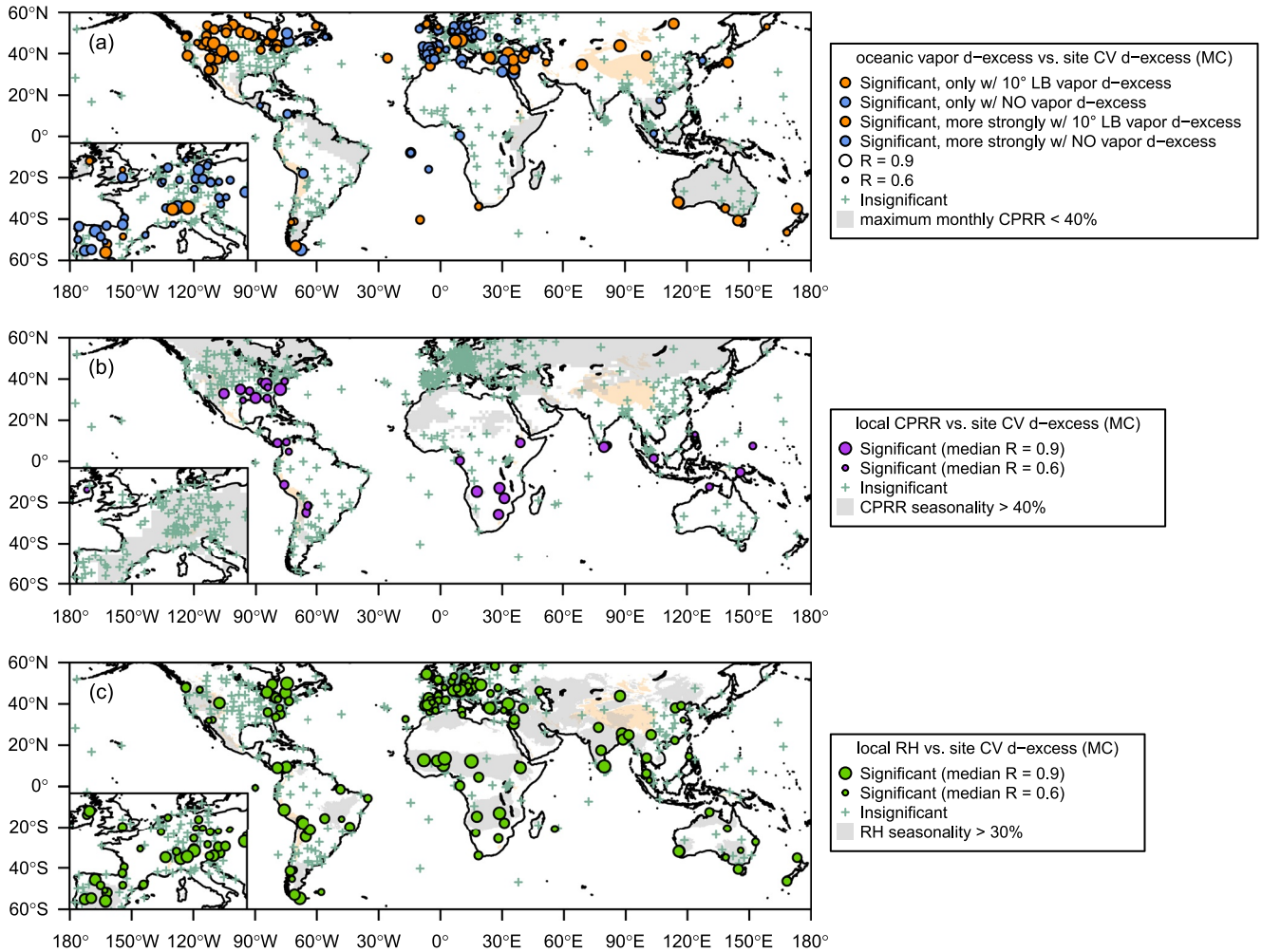

Figure 5. The maps show the spatial distributions of GNIP/USNIP stations where the site CV d-excess has significantly positive Monte Carlo (MC) correlations with the (a) oceanic vapor d-excess, (b) local continental precipitation recycling ratio (CPRR), and (c) local relative humidity (RH), with zoom-ins for Europe. The dot sizes indicate the MC median *R* values. In (a), the orange and blue dots indicate significant correlations with 10° latitudinal band (LB) and nearest ocean (NO) vapor d-excess, respectively. The dots with thicker outlines mean that the CV d-excess has significant correlations with both, but the correlation is stronger (higher MC median *R* value) with 10° latitudinal band (orange) or nearest ocean (blue) vapor d-excess. Gray color areas indicate where the maximum monthly continental precipitation recycling ratio (CPRR) is <40%, suggesting dominant moisture sources from oceans. In (b), gray color areas indicate where the CPRR seasonality is >40%, suggesting intense swings in seasonal moisture recycling. In (c), gray color areas indicate where the RH seasonality is >30%, suggesting a strong hydroclimate seasonality.

such dramatic changes in the continental water cycle, the increased contribution of recycled moisture to the atmospheric water vapor appears not strongly or even not necessarily to increase the precipitation d-excess in continental interiors (Figure 6). Otherwise, we expect to find widespread positive correlations between local CPRR and site CV d-excess. This finding requires a more updated theory to link d-excess with moisture recycling (Wei & Lee, 2019) and is addressed in Section 6. Even for those sites with significant correlations between local CPRR and site CV d-excess, some also exhibited significant correlations between local RH and site CV d-excess (discussed below), as there is a typical in-phase relationship between local CPRR and RH in low-latitudes (Figure S2a in Supporting Information S1).

Significantly positive MC correlations between local RH and site CV d-excess are found in many stations in both low-latitudes and mid-latitudes (Figure 5c). The empirical correlation between local RH and precipitation d-excess on seasonal time scales has been previously found in site-specific studies in different parts of the world (e.g., Crawford et al., 2017; Kaseke et al., 2018; Liebminger et al., 2006). Our new analysis further reveals the prevalence of this finding that underscores raindrop re-evaporation as a potentially simple, widely applicable mechanism underlying the d-excess seasonality in precipitation stations. The correlations are strongest around the

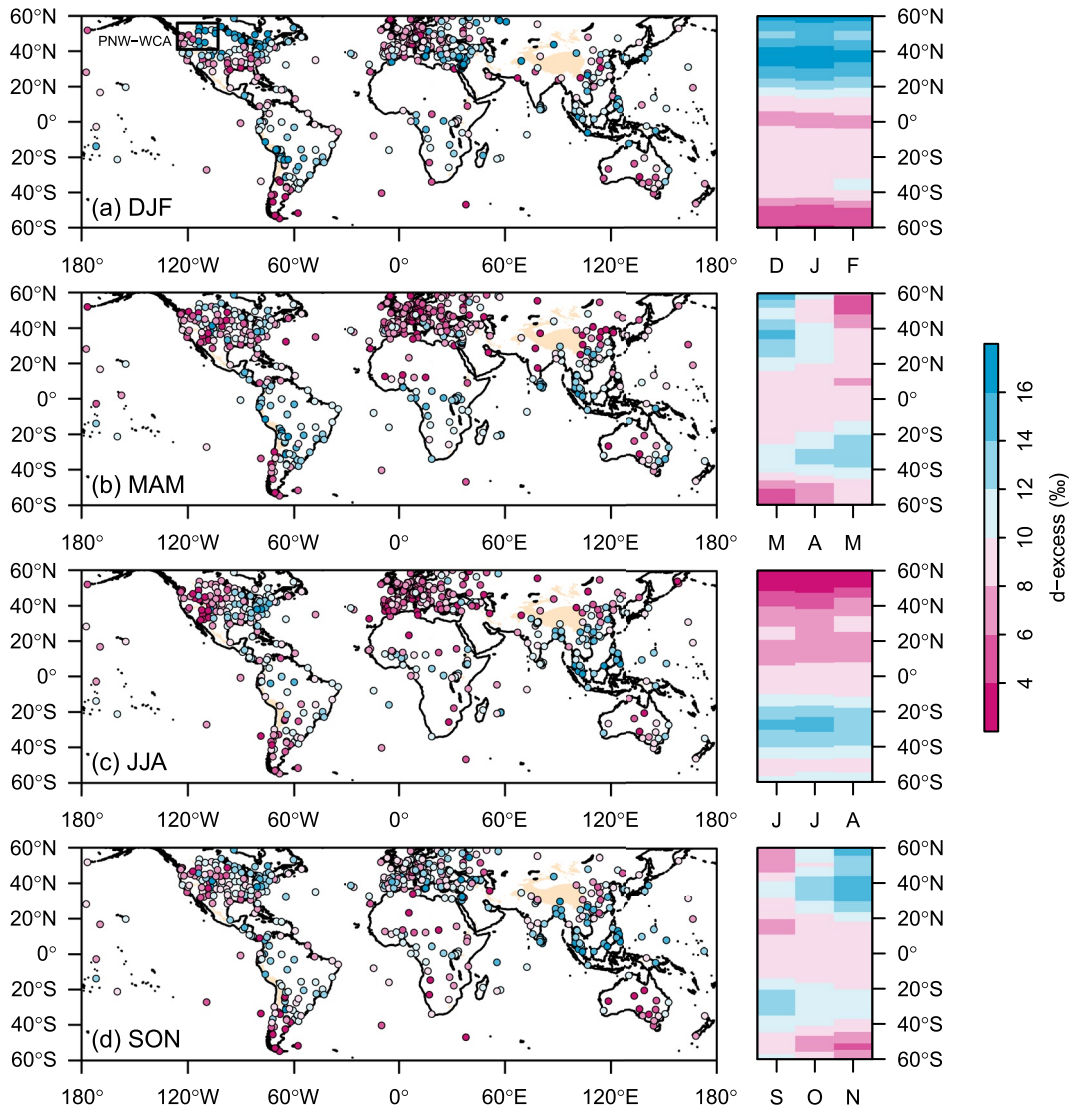

Figure 6. The seasonal mean CV d-excess from GNIP/USNIP stations are shown in colors. On the right side, we show for comparison the monthly means of 10° latitudinal band vapor d-excess as in Figure 1d. The black box in (a) indicates the area of the Pacific Northwest-western Canada (PNW-WCA) transect.

migration boundary of ITCZ where the local hydroclimate is highly seasonal (gray areas in Figure 5c). However, this finding is in contrast to a GCM-based study showing that raindrop re-evaporation controls only to a small extent the seasonality in precipitation d-excess in low-latitudes (Risi et al., 2013). On the other hand, the CV d-excess in many mid-latitude stations is correlated with both the oceanic vapor d-excess and local RH (Figures 5a and 5c). This arises from the fact that seasonally there is an anti-phase relationship between 10° latitudinal band oceanic RH and continental RH in Northern Hemisphere mid-latitudes where most GNIP/USNIP stations are located (Figure S2b in Supporting Information S1), which exert controls on d-excess in the same direction.

These spatial correlation patterns provide an empirical view on the potential drivers of d-excess seasonality in precipitation stations. Importantly, correlations only indicate their coherent phase in variations but do not necessarily imply causation and it is challenging to separate the relative contribution of different drivers. In Section 5, we focus on the 16 representative sites with the WAM-2layers moisture source diagnostics, in which the oceanic source vapor d-excess is directly quantified, to address these open questions.

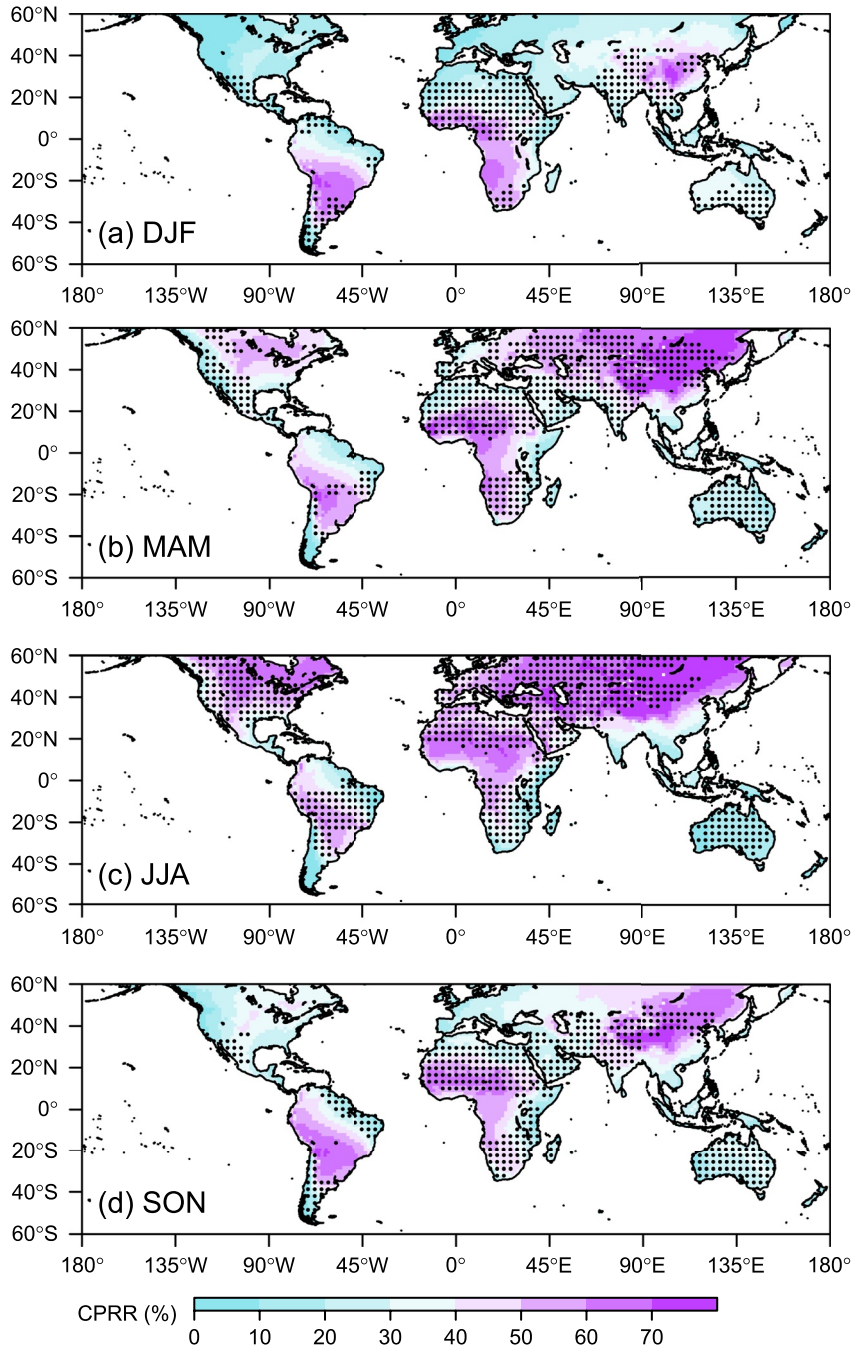

Figure 7. The maps of seasonal mean continental precipitation recycling ratio (CPRR) are shown in colors. The dotted shades are areas with negative surface water balance ($P < ET$) based on precipitation and evapotranspiration (ET) fluxes in ERA5 reanalysis. Note that we find $P < ET$ annually for some very dry areas, reflecting biases in land surface models used in ERA5. The overall pattern is still similar when using other ET products, e.g., the Global Land Evaporation Amsterdam Model (GLEAM; Martens et al., 2017).

5. Discussion on the Diverse Drivers of d-Excess From Site-Specific Analyses

5.1. The Effect of Oceanic Source Vapor

The 12 monthly tracked evaporation fractions for 16 representative sites of moisture source diagnostics are presented in Movies S1 (with terrestrial evaporation) and S2 (without terrestrial evaporation), which show seasonal changes in moisture source regions. Comparing the oceanic vapor d-excess of diagnosed moisture

source regions with the site CV d-excess in moisture sink regions allows us to directly validate the well-known oceanic moisture source effect on d-excess.

The diagnosed oceanic source vapor d-excess shows an overall similar seasonal pattern with the respective 10° latitudinal band vapor d-excess for all nonequatorial sites, but not so with the nearest ocean vapor d-excess (Figures 2 and 3). Two inferences can be drawn from these comparisons. First, on seasonal time scales, oceanic source vapor d-excess for these representative sites largely follows the hemisphere-wide shift in oceanic RH regardless of changes in moisture source regions. Second, evaporation conditions over the nearest ocean do not accurately represent the conditions of actual moisture source regions even though some sites may exhibit significant correlations between nearest ocean vapor d-excess and site CV d-excess as shown in Figure 5a. There are many such sites in the north of the European Alps where the nearest ocean (mostly the North Sea) vapor d-excess seems highly coherent with the CV d-excess, such as Artern in Germany (Figure 3c), but moisture source diagnostics indicate high contributions of moisture sources from North Atlantic (Movie S2). As for equatorial sites, the diagnosed oceanic source vapor d-excess has two semiannual cycles in São Gabriel da Cachoeira of Brazil (within the Amazon rainforest) and Bangui of Central African Republic (Figures 2c and 3e), a pattern that has been previously predicted as these areas receive moisture from subtropical highs twice a year following the migration of ITCZ (Feng et al., 2009). However, Belem (northern Brazil) has a Southern Hemisphere-like seasonality without semiannual cycles (Figure 2d).

As for comparisons with the CV d-excess of these 16 representative sites, we find that in eight sites there is no apparent source-sink coherency in d-excess: Buenos Aires, Cuiabá (Brazil), Belem, Caddo Valley, Bangui, Tianjin (northern China), Hong Kong, and Brisbane (Figures 2 and 3). All these sites are in the tropics and subtropics except Tianjin. A simple explanation for the incoherency is that other major processes, such as raindrop re-evaporation and moisture recycling that are discussed later, have altered the d-excess signal of oceanic source vapor. This also may in part be a result of weaker d-excess seasonality of oceanic vapor in low-latitudes. For other sites with the source-sink coherency in d-excess, it is insufficient to pinpoint oceanic evaporation conditions as the sole mechanism and exclude other processes in producing the observed seasonality of site CV d-excess. Using Ankara as an example, although the CV d-excess shows a strong coherency with the diagnosed oceanic source vapor d-excess, both having an amplitude of variations of about 8‰, it shows a strong coherency with the local RH as well which controls the degree of raindrop re-evaporation (Figure 3d). The lowest CV d-excess occurs in July–August when local RH also reaches the lowest values, while the diagnosed oceanic source vapor d-excess has the lowest values in June, in part reflecting the evaporation conditions over the Mediterranean ocean basin (Figures 1b and 3d).

Besides evaluating the phase coherency in d-excess, we note that all these sites show systematic residuals between diagnosed oceanic source vapor d-excess and site CV d-excess values (Figures 2 and 3). These suggest that the conservation of d-excess from oceanic sources to continental sinks should not be taken for granted and that subsequent modifications of oceanic source vapor are crucial to determine the d-excess observed in continental precipitation. We calculate their root mean square (RMS) residuals as

$$\mathrm{RMS} = \sqrt{\frac{\sum (d_{s,i} - d_{cv,i})^2}{n}} \tag{10}$$

where $d_{s,i}$ and $d_{cv,i}$ are the diagnosed oceanic source vapor d-excess and site CV d-excess for month i (1, 2, 3, …, 12), respectively, and $n = 12$ (except Tianjin where $n = 11$ with one monthly gap). Among the 16 representative sites, it is found that the RMS residual becomes larger for sites with lower annual mean RH and higher maximum monthly CPRR (Figure 8). This finding implies that for more arid and inland areas with stronger raindrop re-evaporation and more intense seasonal swings in moisture recycling, there is indeed an increasing degree of modifications on d-excess from the signal of oceanic source vapor, consistent with the conclusion of a previous study using direct water vapor d-excess measurements at three comparative sites (Wei & Lee, 2019).

Still, for sites in humid and coastal areas, the RMS residual is at least 2‰ and some individual monthly d-excess residuals are even larger (Figures 2, 3, and 7). For example, the CV d-excess in Saturna (British Columbia, Canada) and Artern is about 5‰ lower in DJF (Figures 2h and 3c), while in Hong Kong is about 5‰ higher in JJA (Figure 3g), than their respective diagnosed oceanic source vapor d-excess. These sites all have high RH (>80%) and low CPRR (<20%) and thus it is unlikely that the effects of raindrop re-evaporation and moisture

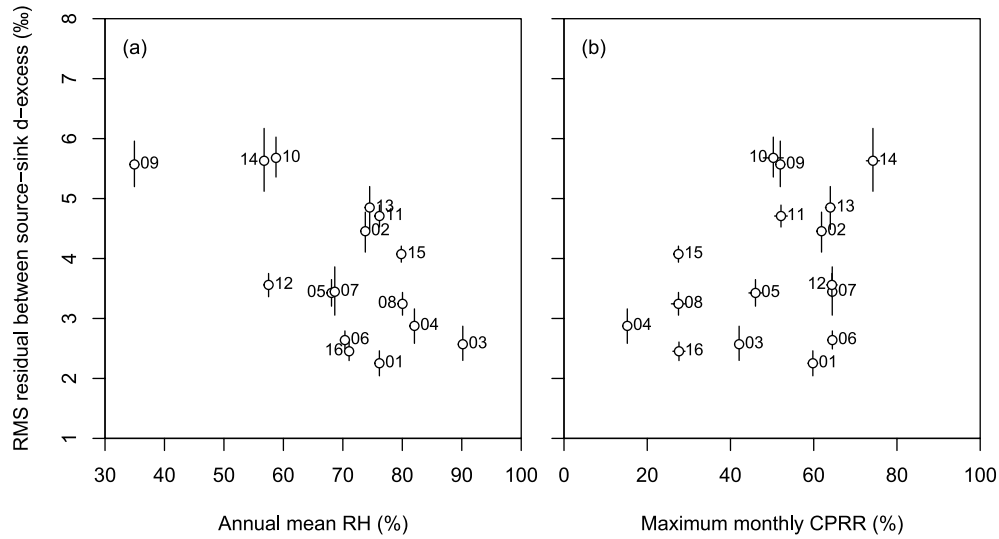

Figure 8. Median root mean square (RMS) residuals between diagnosed oceanic source vapor d-excess and site CV d-excess and their relationships with (a) annual mean relative humidity (RH) and (b) maximum monthly continental precipitation recycling ratio (CPRR). The error bars for RMS residuals represent the 25% and 75% quartiles in 10^4 MC sampling, and for RH and PCRR are their standard error of the means (SEMs) that are typically smaller than the dot sizes. Number labels for each data point correspond to Table 1.

recycling are strong enough to explain the large d-excess residuals in the respective period. These large monthly d-excess residuals are not local features but indicate distinct regional anomalies we have identified in the seasonal mean CV d-excess map (Figure 6). Again, the Pacific coast of North America as well as western Europe have lower CV d-excess than both the latitudinal means as well as further inland areas in DJF (Figure 6a). The Southeast Asia sites have high CV d-excess in JJA when summer monsoon dominates (Figure 6c).

From these source-sink comparisons of d-excess, we infer that the oceanic moisture source effect on d-excess is dominant in mid-latitudes based on the temporal coherence, but the contributions from other processes cannot be excluded, which we aim to address in following sections. The oceanic moisture source effect in low-latitudes, however, does not dominate the d-excess seasonality, with a possible exception from the Amazon rainforest (Figure 2c). A quantification of source-sink d-excess residuals supports the view that there is an increasing isotopic modification on the oceanic source vapor in more arid and inland areas, but it remains to be explained why d-excess residuals are still large in wet and coastal areas. We hypothesize that these residuals may be the product of prior distillations in contributing air masses over oceans, which do not conserve the d-excess. To test this hypothesis, we next explore the direction and magnitude of changes in d-excess under the idealized Rayleigh distillation process.

5.2. The d-Excess Variability in Rayleigh Distillation

The primary assumption underlying d-excess as a metric of kinetic fractionation in the hydrological cycle is that there is a ratio of 8:1 between the change in δ^2H and $\delta^{18}O$ in equilibrium phase change reactions (Dansgaard, 1964). Under Rayleigh distillation, whereby condensate is continuously removed from an idealized mass of cooling water vapor, the isotopic compositions of vapor (δ_v) and precipitation (δ_p) follow:

$$\delta_v = (\delta_{v,0} + 1,000)\, f^{\alpha-1} - 1,000 \tag{11}$$

and

$$\delta_p = \alpha(\delta_{v,0} + 1,000) f^{\alpha-1} - 1,000 \,(\text{Dansgaard, 1964}) \tag{12}$$

where $\delta_{v,0}$ is the initial isotopic composition of vapor, f is the fraction of remaining vapor, and α again is the fractionation factor which includes kinetic components when $T_d < 0$ °C (see Section 2.1).

Mathematically, the slope of the relationship between δ^2H and $\delta^{18}O$ in vapor at a certain moment of Rayleigh distillation is

$$\frac{d\delta^2H}{d\delta^{18}O} = \frac{\alpha_2 - 1}{\alpha_{18} - 1} \times \frac{\delta^2H + 1,000}{\delta^{18}O + 1,000} \text{ (Dütsch et al., 2017)} \quad (13)$$

where α_2 and α_{18} refer specifically to the fractionation factor for δ^2H and $\delta^{18}O$, respectively. Conservation of d-excess in vapor under Rayleigh distillation is therefore only valid when the right-hand side of this equation equals 8. For $T_d > 0$ °C, the term $\frac{\alpha_2 - 1}{\alpha_{18} - 1}$ is around 8 only when T_d is as high as 37 °C and increases to 9.6 when T_d decreases to 0 °C. The term $\frac{\delta^2H + 1,000}{\delta^{18}O + 1,000}$ is <1 because δ^2H is generally more negative than $\delta^{18}O$, and this term decreases further under decreasing T_d as δ^2H is depleted to a larger degree than $\delta^{18}O$. These two terms thus compensate for each other in response to air mass cooling such that their product is close to 8, which explains the consistent slope of the Global Meteoric Water Line. Still, under certain conditions, these two terms, which have been referred to as the δ-scale effect and temperature effect, respectively (Dütsch et al., 2017), lead to the deviation of $\frac{d\delta^2H}{d\delta^{18}O}$ from 8 and thereby alter d-excess under Rayleigh distillation. For $T_d < 0$ °C, kinetic effects due to supersaturation over ice also contribute to govern $\frac{d\delta^2H}{d\delta^{18}O}$ (Dütsch et al., 2019; Jouzel & Merlivat, 1984).

To quantify how much change in vapor d-excess will occur by Rayleigh distillation, we develop idealized modeling experiments by varying the initial T_d and vapor $\delta^{18}O$, which determine the balance between the δ-scale and temperature effects in the given Rayleigh system. For this analysis, the initial vapor d-excess is set to 10‰. The total distillation and T_d are linked by the Clausius-Clapeyron relation

$$e_s = 611.2 \exp\left(\frac{17.67T_d}{T_d + 243.5}\right) \text{ (Bolton, 1980)} \quad (14)$$

where e_s is saturation vapor pressure (in Pa). For each cooling step, fractionation factors and f are updated (Dütsch et al., 2017). Similar "simple isotope model" experiments have been explored extensively to understand the evolution of d-excess signals in polar snow and ice (e.g., Ciais & Jouzel, 1994; Delmotte et al., 2000; Dütsch et al., 2019; Johnsen et al., 1989; Jouzel & Merlivat, 1984; Landais et al., 2008; Petit et al., 1991), but our interest is in the change in vapor d-excess in non-polar regions where the temperature is relatively higher. This analysis also relates to the d-excess offset between vapor and precipitation we have explored in Section 3; the change in vapor d-excess during Rayleigh distillation reflects the consequence of this offset in the progressive removal of condensate from water vapor.

Figure 9a shows the changes in vapor d-excess under a range of initial conditions in T_d and vapor $\delta^{18}O$ as contour lines when Rayleigh f reaches 0.4, corresponding to a 60% total distillation. The results when Rayleigh f is 0.6 or 0.2 are shown in Figure S3 in Supporting Information S1 for comparison. As described above, higher initial T_d and lower initial vapor $\delta^{18}O$ values generally result in increases in vapor d-excess during Rayleigh distillation, and vice versa (Figure 9a), and the magnitude of these increases or decreases becomes larger with greater degrees of distillation (Figure S3 in Supporting Information S1). The "upward shift" of zero contour lines as Rayleigh f decreases from 0.6 to 0.2 indicates that under certain initial conditions, vapor d-excess may at first decrease at high f values and then increase at low f values. When Rayleigh $f = 0.2$, Figure S3 in Supporting Information S1 also shows that Rayleigh distillation alone may induce vapor d-excess changes of >10‰ under extreme initial conditions. Again, the parameterization of mixed-phase clouds and supersaturation conditions impacts the results when distillation reaches subfreezing temperatures and may lead to a deviation of up to 6‰ when Rayleigh $f = 0.2$ (Figure S3 in Supporting Information S1).

To constrain a reasonable space between initial vapor $\delta^{18}O$ and T_d in observations, we also plot in Figure 9a the distribution of monthly mean CV $\delta^{18}O$ and T_d in warm (i.e., JJA for Northern Hemisphere and DJF for Southern Hemisphere) and cold seasons from non-arid (RH > 70%), coastal (distance to oceans <100 km) GNIP/USNIP stations. We exclude equatorial stations ($T_d > 20$ °C) for cold seasons. We assume that sites in wet and coastal areas provide a snapshot of the realistic combinations of initial vapor $\delta^{18}O$ and T_d that establish Rayleigh distillation in the respective season. Using the case of Rayleigh $f = 0.4$ as an example, we find that many warm-season data plot below the zero contour line within the space where Rayleigh distillation increases d-excess. By contrast, most cold-season data plot above the zero contour line within the space where Rayleigh distillation decreases

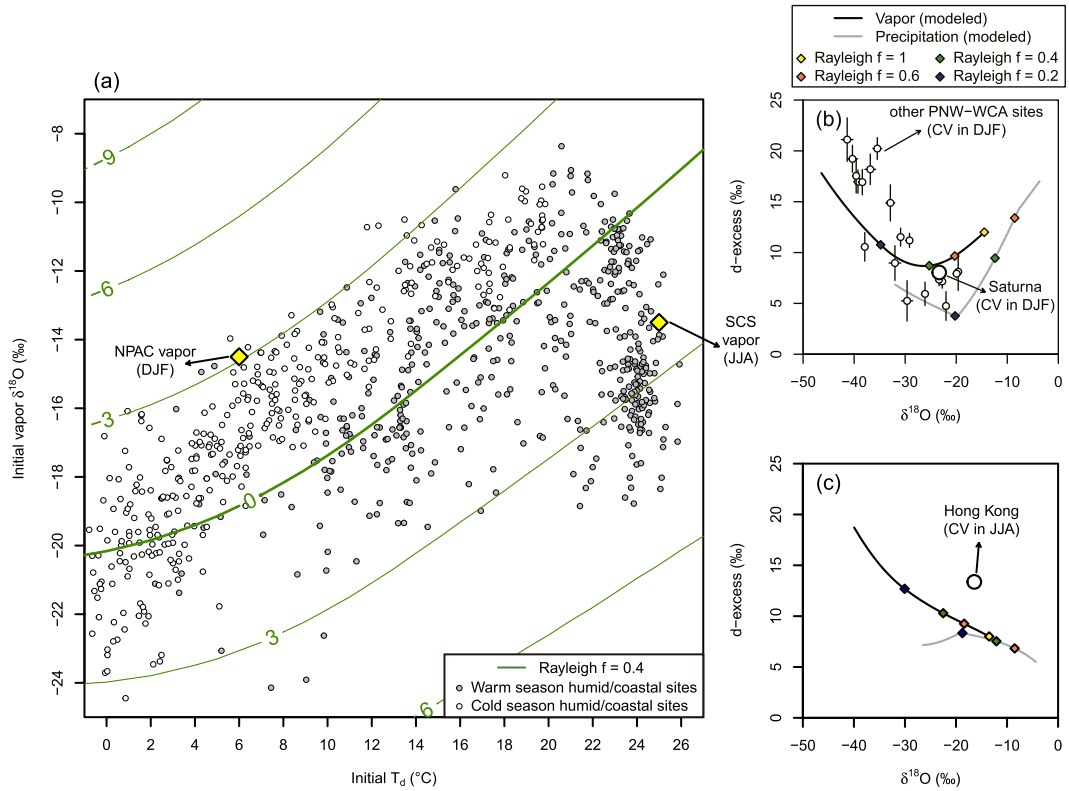

Figure 9. (a) Changes in vapor d-excess under Rayleigh distillation are shown in green contour lines given a range of initial conditions in T_d and vapor $\delta^{18}O$ when Rayleigh f is 0.6. Also shown are scatter points of monthly mean CV $\delta^{18}O$ observations and ERA5 monthly mean T_d during warm (gray dots) and cold (white dots, with $T_d < 20$ °C) seasons from non-arid (relative humidity > 70%), coastal (distance to oceans <100 km) GNIP/USNIP stations to constrain the possible space in initial conditions. Yellow diamonds are the LMDZ4-based initial conditions for the North Pacific (NPAC) in DJF and the South China Sea (SCS) in JJA. (b) Modeled changes in $\delta^{18}O$ and d-excess for vapor (black line) and precipitation (gray line) under Rayleigh distillation based on the initial conditions of the North Pacific in DJF. Colored diamonds mark the degree of distillation. Also shown are the isotopic compositions of CV in Saturna (large dot) and other sites from the Pacific Northwest-western Canada (PNW-WCA) transect in DJF (Figure 6a). The error bars represent standard error of the means (SEMs). (c) Similar to (b) but initial conditions are based on the South China Sea and the data point is from Hong Kong in JJA.

d-excess. As far as the amplitude of d-excess changes is concerned, most of the data are bounded within the contour lines of ±3‰ (Figure 9a).

The analysis of Rayleigh distillation with observational constraints on initial conditions suggests that up to 3‰ or even larger variations in d-excess are likely to occur by Rayleigh distillation alone, and the direction of change depends on the season and the degree of distillation. This finding provides a simple explanation for the lower CV d-excess in Saturna and Artern in DJF than their respective diagnosed oceanic source vapor d-excess, as discussed above, because prior distillations over oceans decrease the vapor d-excess. Indeed, North Pacific and North Atlantic oceans are known for the high frequency of storm activity and abundant oceanic precipitation in winter due to the intensification of cyclonic circulation (Hurrell & Deser, 2010; Serreze et al., 1997; Simmonds & Keay, 2002). In addition, in both North America and Eurasia, we observed increases in CV d-excess along continental westerly flows (Figure 6a). Because subfreezing temperatures in these locations limit moisture recycling and raindrop re-evaporation, these spatial changes in CV d-excess are likely induced by Rayleigh distillation as well. These are also consistent with the previous finding that vapor d-excess may shift from decreasing to increasing values as distillation proceeds further. To visualize these changes, we plot in Figure 9b the Rayleigh distillation curves established from initial vapor $\delta^{18}O$ of −14.5‰ and T_d of 6 °C, which represent the vapor source conditions over the North Pacific ocean basin in DJF based on the output of nudged isotope-enabled GCM LMDZ4 (Risi et al., 2010, 2012). The initial vapor d-excess is set to 12‰ (Figures 2g and 2h). The results are compared to the DJF mean CV $\delta^{18}O$ and d-excess data from sites within the Pacific Northwest-western Canada

transect (Figure 6a), where the dominant moisture source is the North Pacific (Movie S2). Although the Rayleigh distillation model does not resolve the mixing by turbulent eddies or with other moisture sources (Winnick et al., 2014), it reproduces the coupled changes in vapor $\delta^{18}O$ and d-excess, including lower CV d-excess in Saturna than the oceanic source vapor upon arrival at western North America and higher CV d-excess at downstream inland locations (Figure 9b).

By contrast, in Hong Kong, higher CV d-excess values than oceanic source vapor d-excess in JJA are not well explained by simple Rayleigh distillation. Using the vapor source conditions over the South China Sea (Cai et al., 2018), a 5‰ increase in vapor d-excess requires a very large degree of distillation that produces very low $\delta^{18}O$ inconsistent with observations (Figure 9c). In fact, the isotopic composition of precipitation in Hong Kong and its adjacent regions is strongly controlled by monsoon convection (Cai & Tian, 2016; Cai et al., 2018; Wei et al., 2018). Specifically, the lower precipitation $\delta^{18}O$ in JJA in Hong Kong (Figure 4) and across broad Asian monsoon-dominated areas is produced by stronger tropical convective activity, which is increasingly fed by high-level vapor injected into the boundary layer through downdrafts and affected by other raindrop-vapor interactions (Risi et al., 2008). A combination of multiple processes and feedbacks in convective systems together determine the vapor and precipitation $\delta^{18}O$ that are often known as the isotopic "amount effect," the negative correlation between precipitation amount and precipitation $\delta^{18}O$ (Bony et al., 2008; Risi et al., 2008), and these signals are advected to monsoon-dominated areas (Cai et al., 2018). It has been shown in single-column models that the same "amount effect" mechanism should also result in higher d-excess values under stronger convective activity (Bony et al., 2008). Therefore, the higher CV d-excess in Hong Kong and Southeast Asia (Figure 6c) may be the product of complex interactions in monsoon convection, which do not conform to Rayleigh distillation. Interestingly, Cai and Tian (2016) have expected to find higher d-excess in Asian monsoon-dominated areas in JJA based on the characteristics of convective systems, but suggested instead that the d-excess is higher in DJF based on RP d-excess data. We note that the RP d-excess in Hong Kong has an in-phase relationship with the diagnosed oceanic source vapor d-excess (Figure 3g), which seems to support the oceanic moisture source effect. However, the CV d-excess, which has an opposite seasonal pattern, does not support this effect but is instead consistent with the effect of convective activity as originally hypothesized by Cai and Tian (2016). This shows the importance of correcting the local condensation effect in d-excess data to effectively identify the process-based mechanism for d-excess seasonality.

Overall, we show that vapor d-excess is not conserved under Rayleigh distillation, a fact that highlights the complexity of using d-excess as a tracer of oceanic moisture source conditions even in coastal areas and without considering other processes. An application of Rayleigh distillation reproduces observed changes in vapor d-excess across western North American vapor transport paths in winter, but not in Southeast Asia where and when regional convective activity is dominant.

5.3. The Effect of Raindrop Re-Evaporation

Our previous work using a model of raindrop re-evaporation shows that surface RH, by controlling the lifting condensation level, is the key factor to determine the subcloud modifications on the isotopic composition of raindrops over time scales longer than individual precipitation events (Graf et al., 2019; Xia & Winnick, 2021). As local RH becomes higher, raindrop d-excess decreases to a lesser extent due to the shorter falling times of raindrops, and vice versa. This conclusion assumes that raindrops are formed and released at the cloud base and that the unsaturated subcloud vapor is in isotopic equilibrium with initial raindrops. In tropical convective systems where vertical motion and mixing are important, these assumptions poorly represent reality (Risi et al., 2008). However, the relationship between surface RH and precipitation d-excess is qualitatively similar. Higher local RH co-occurs with higher precipitation rates under stronger convective activity that increases the flux and recycling of downdraft water vapor, decreases the raindrop re-evaporation, and ultimately increases the d-excess in precipitation in convective systems (Bony et al., 2008; Risi et al., 2008). We consider local RH as an integrated metric to measure the effect of raindrop re-evaporation on d-excess that may, in part, be linked to the regional convective activity.

Among the 16 representative sites, in Cuiabá, Bangui, and Tianjin with strong hydroclimate seasonality, and even in coastal sites Belem, Hong Kong, and Brisbane where seasonal variations in RH are smaller, it is apparent that local RH shows a strong coherency with site CV d-excess and has entirely overprinted the seasonal pattern of diagnosed oceanic vapor source d-excess (Figures 2 and 3). For other sites in mid-latitudes where the CV

d-excess is temporally coherent with both the diagnosed oceanic source vapor d-excess and local RH, we still find evidence for potential modifications of local RH on CV d-excess. Specifically, the lowest CV d-excess in Ottawa occurs in April–May when the local RH, not the diagnosed oceanic source vapor d-excess, also reaches the lowest values (Figure 2f), and likewise in May–June in much drier Tucson (Figure 3a) and in July–August in Ankara mentioned in Section 5.1 (Figure 3d). In Saskatoon (western Canada), two periods of lower RH in April–May and August–September coincide with two periods of relatively lower CV d-excess (Figure 2g). In Ciudad Real (Spain), the CV d-excess is distinctly lower in the driest JJA when the diagnosed oceanic source vapor d-excess only shows a moderate decrease (Figure 3b).

From these mid-latitude sites, we suggest that the combined effects of oceanic source vapor d-excess and local RH that are in-phase may amplify the response of site CV d-excess in observations. For example, the amplitude of seasonality in diagnosed oceanic source vapor d-excess is about 5‰ in Tucson and 7‰ in Ciudad Real, but the amplitude of seasonality in CV d-excess is about 12‰ for both sites (Figures 3a and 3b). Therefore, separating the individual contribution of oceanic moisture source and raindrop re-evaporation effects seems possible. However, we also find cases where the combined effects of oceanic moisture source and raindrop re-evaporation do not cause an amplified response in CV d-excess. In Artern and Ankara, the amplitude of seasonality in diagnosed oceanic source vapor d-excess is about 8‰, but the amplitude of seasonality in CV d-excess is about 5‰ and 8‰, despite the in-phase seasonal changes in local RH of 20% and 40%, respectively (Figures 3c and 3d). In other words, the enhanced raindrop re-evaporation in dry summers does not result in even lower site CV d-excess. We suggest two possible reasons for this lack of amplification. The first mechanism is the season-dependent change in vapor d-excess by Rayleigh distillation over oceans we have discussed in Section 5.2. As initial conditions in winter and summer tend to result in the decrease and increase in vapor d-excess during the distillation (Figure 9a), respectively, these in turn may reduce the seasonal contrast in vapor d-excess observed at a specific site. The second and potentially more important mechanism is the substantial shift in continental moisture recycling in mid-latitudes (Figure 7), such as in Ankara where CPRR increases from <10% in DJF to 60% in JJA (Figure 3d). If moisture recycling in summer has replenished the atmospheric water vapor with a flux of relatively higher d-excess vapor, it may compensate for the strong raindrop re-evaporation effect that decreases the d-excess in precipitation. Validating these dynamics requires a thorough understanding of the d-excess signal in ET fluxes and will benefit from coupled isotopic measurements of water vapor and precipitation (Aemisegger et al., 2014; Bonne et al., 2020; Conroy et al., 2016; Kurita & Yamada, 2008).

Overall, we use the analysis of representative sites to further support that the raindrop re-evaporation effect, as indicated by local RH, exerts a dominant control on CV d-excess and overprints the oceanic moisture source effect in low-latitudes. It is still important in mid-latitudes and modulates the seasonal pattern in CV d-excess, such as determining the month of lowest d-excess and amplifying the amplitude of d-excess seasonality at some sites.

5.4. Summary

Using moisture source diagnostics that allow us to quantify the d-excess signal of oceanic source vapor, we use several representative GNIP/USNIP stations as examples to demonstrate that the precipitation d-excess seasonality in continental locations is controlled by compound mechanisms. We find that the raindrop re-evaporation effect, which may be linked to regional convective activity in the tropics, dominates over the oceanic moisture source effect in low-latitude sites. However, the drivers of precipitation d-excess seasonality in mid-latitude sites are more complex. Our analysis does not invalidate the oceanic moisture source effect, which becomes stronger at higher latitudes, as the main mechanism for d-excess seasonality in mid-latitudes as indicated by spatial correlation patterns. However, prior distillations over oceans, seasonal swings in moisture recycling, and local raindrop re-evaporation all act to modify the d-excess signal of oceanic source vapor. We suggest that these source-route-sink effects exert a complex control on observed d-excess signals in continental precipitation and challenge the accuracy of d-excess as a simple tracer for oceanic moisture source conditions.

6. The Effect of Moisture Recycling on d-Excess

Moisture recycling via ET is ubiquitous over continents and a fundamental component of the water cycle and climate system. ET fluxes return about 2/3 of continental precipitation to the atmosphere (Trenberth et al., 2011), and over 1/3 of continental precipitation itself is supplied by this recycled moisture (van der Ent et al., 2014). Certainly, moisture recycling should have a profound effect on the spatial and temporal distribution of isotope species in the water cycle (Winnick et al., 2014). Based on current knowledge, the kinetic fractionation in diffusive transport of water vapor results in higher d-excess in evaporation fluxes than surface source water (Craig & Gordon, 1965), while plant-mediated transpiration fluxes are often considered to not fractionate relative to the plant source water on longer than daily time scales, thus conserving $\delta^{18}O$ and d-excess (Flanagan et al., 1991). Still, moisture recycling is often invoked, without distinguishing the component of evaporation and transpiration in ET, as a simple mechanism to reduce the spatial gradient in precipitation $\delta^{18}O$ relative to Rayleigh distillation over continents (Liu et al., 2010; Mix et al., 2013; Salati et al., 1979) and to increase the precipitation d-excess toward continental interiors due to the admixture of evaporated moisture with the atmosphere (Ampuero et al., 2020; Gat & Matsui, 1991; Taupin et al., 2000).

In Section 5.3, we have proposed that the enhanced moisture recycling in summer may increase the vapor d-excess that, in part, compensates for the concurrent stronger raindrop re-evaporation in Ankara (Figure 3d). Among other representative sites, in São Gabriel da Cachoeira within the Amazon rainforest, the CV d-excess is about 3‰ higher than the diagnosed oceanic source vapor d-excess in July–October when the CPRR is highest, and is only about 1‰ higher than the diagnosed oceanic source vapor d-excess in January–March when the CPRR is lowest (Figure 2c). In Caddo Valley, the CV d-excess shows a strong phase coherency with the CPRR and is about 4‰ higher than the diagnosed oceanic source vapor d-excess in high-CPRR JJA (Figure 2e). These examples do seem to support the view that the increased recycled moisture in the atmosphere is expressed by higher d-excess if other processes are not considered. Regardless, the spatially limited correlation patterns between local CPRR and site CV d-excess (Figure 5c) suggest that the moisture recycling effect that presumably increases the vapor d-excess in continental interiors is too weak to dominate the d-excess seasonality in mid-latitudes despite large changes in CPRR (Figure 7).

In this section, we focus on why large seasonal swings in moisture recycling in mid-latitudes do not introduce strong d-excess responses. We provide two hypotheses for the complexity of the relationship between moisture recycling and d-excess over continents. First, the warm and high-CPRR season in the Northern Hemisphere generally occurs during widespread negative water balance conditions: i.e., more ET outflux than precipitation influx ($P < ET$) over North America and Eurasia (Figure 7c). This implies that a considerable proportion of terrestrial ET in this dry (i.e., $P < ET$) season is supplied by the residual water storage of the previous wet season when a net recharge ($P > ET$) occurs. Thus, the ET flux inherits the low, evaporation-impacted d-excess signal of this residual water storage. Second, nonfractionating plant transpiration might be the major pathway of moisture recycling in the warm and dry, high-CPRR season, by which d-excess is not significantly impacted by the contribution of recycled moisture. To test these two hypotheses, we describe an idealized model that accounts for the seasonal water storage and ET partitioning effects to predict the isotopic composition of ET fluxes (δ_{ET}) in Section 6.1. We use simple model experiments to demonstrate the model behaviors and fundamental mechanisms in Section 6.2. We then briefly discuss the implications in Section 6.3.

6.1. The Seasonal Water Storage Model for δ_{ET}

In our previous study, we developed a simple parameterization for δ_{ET} with the implementation of the "closure assumption" and Rayleigh distillation-type progressive removal of liquid water as

$$\delta_{ET} = \left(\frac{E}{ET}\right)\frac{\int_1^F \left[\alpha_{ET}(\delta_I + 1{,}000)F^{\alpha_{ET}-1} - 1{,}000\right]dF}{F-1} + \left(\frac{T}{ET}\right)\delta_I \text{ (Xia \& Winnick, 2021)} \quad (15)$$

where $\frac{E}{ET}$ and $\frac{T}{ET}$ are the surface evaporation and plant transpiration fraction of ET, respectively, F is the fraction of residual liquid water remaining after ET loss expressed as $(P - ET)/P$. The capitalized symbol F distinguishes from the symbol f in Section 5.2, both of which describe the remaining fraction in Rayleigh-based models. δ_I is the isotopic composition of precipitation input and α_{ET} is the apparent fractionation factor of evaporation that through the "closure assumption" is affected by the concurrent transpiration flux as

$$\alpha_{ET} = \left(\frac{E}{ET}\right)\left[k\frac{\alpha_{eq}^{v-l}}{(1-h)\left(1+k\frac{E}{ET}\frac{h}{1-h}\right)}\right] + \left(\frac{T}{ET}\right)\left(\frac{1}{1+k\frac{E}{ET}\frac{h}{1-h}}\right) \quad (16)$$

where α_{eq}^{v-l} is the vapor-liquid equilibrium fractionation factor ($1/\alpha_{eq}^{l-v}$) and k is the kinetic fractionation factor of evaporation. The factor k can be expressed as $(D'/D)^m$ where D'/D is again the ratio of diffusivities and m is the aerodynamic exponent that controls the ratio of diffusive over turbulent transport of water vapor, which ranges between 0.5 and 1 for terrestrial environments (except large water bodies; Dongmann et al., 1974; Pfahl & Wernli, 2009).

An important feature of this parameterization is the dependence of δ_{ET} on water balance, similar to an earlier steady-state model of evaporation (Gat & Matsui, 1991). Both require that $P > ET$, a reasonable condition over annual time scales. In order to derive δ_{ET} under the $P < ET$ condition, from an isotopic perspective, the terms F and δ_I in Equation 15 should represent contributions of residual water storage, which is neglected in our previous study (Xia & Winnick, 2021).

Here, we refine the model for δ_{ET} by incorporating the seasonal water storage effect with the least extent of necessary complexity; more complex storage mixing and selection parameterizations ("isotope transfer function") have been developed in land surface models for modeling both short-term and long-term δ_{ET} variations (Gat & Airey, 2006; Henderson-Sellers et al., 2006). We only consider two consecutive seasons to represent a year: a wet season with $P > ET$ followed by a dry season with $P < ET$. We write the precipitation, runoff, and ET as P_1, R_1, and ET_1 for the wet season, and P_2, R_2, and ET_2 for the dry season. Given an initial water storage amount S_0, the residual water storage after ET loss for the wet and dry seasons is

$$S_1 = S_0 + P_1 - R_1 - ET_1 \text{ and } S_2 = S_1 + P_2 - R_2 - ET_2 \quad (17)$$

respectively. Assuming that runoff precedes ET, the term F for the wet and dry seasons is

$$F_1 = \frac{S_1}{S_1 + ET_1} \text{ and } F_2 = \frac{S_2}{S_2 + ET_2} \quad (18)$$

respectively. Next, we denote the isotopic composition of these water fluxes and storages with the "δ" symbol. In order to calculate δ_{ET_1} and δ_{ET_2} using Equation 15, we further assume that precipitation-generated runoff loss occurs rapidly without isotopic fractionation. We use the term δ_I to represent the "modified source water" (δ_{I_1} and δ_{I_2}) mixing the new precipitation input after runoff loss with the old residual water storage as

$$\delta_{I_1} = X_1\delta_{S_0} + (1 - X_1)\,\delta_{P_1} \text{ and } \delta_{I_2} = X_2\delta_{S_1} + (1 - X_2)\,\delta_{P_2} \quad (19)$$

where X_1 and X_2 denote the fraction of residual water storage in the source water pool as

$$X_1 = \frac{S_0}{S_0 + P_1 - R_1} \text{ and } X_2 = \frac{S_1}{S_1 + P_2 - R_2} \quad (20)$$

The isotopic composition of residual water storage after ET loss, δ_{S_1} and δ_{S_2}, can be derived using the isotope mass balance as

$$\delta_{S_1} = \frac{\delta_{I_1} - (1 - F_1)\delta_{ET_1}}{F_1} \text{ and } \delta_{S_2} = \frac{\delta_{I_2} - (1 - F_2)\delta_{ET_2}}{F_2} \quad (21)$$

Finally, we force the final storage condition to be consistent with the initial storage condition of the model. That is, the size of residual water storage and its isotopic composition after ET loss for the dry season is the same as the initial condition for the (next) wet season

$$S_2 = S_0 \text{ and } \delta_{S_2} = \delta_{S_0} \quad (22)$$

This boundary condition constraint allows us to determine δ_{S_0} if all other required model inputs (including S_0) are known.

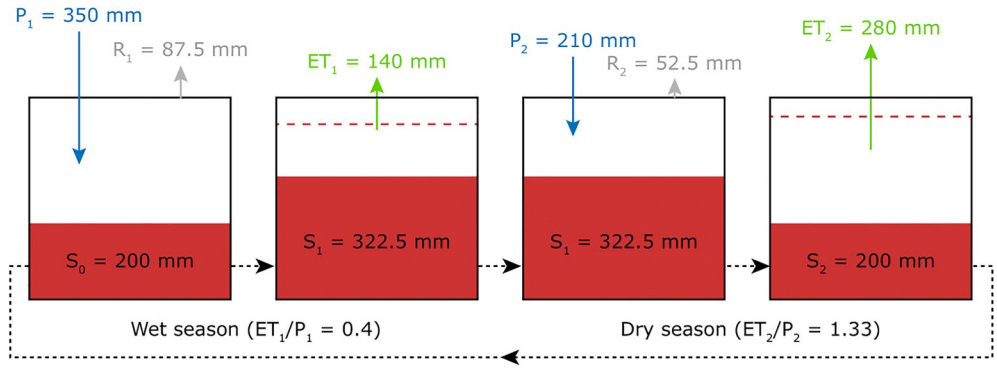

Figure 10. The schematic diagram shows the water fluxes and storages during wet and dry seasons for the simple experiment of the seasonal water storage model.

6.2. Seasonal Water Storage Model Experiments

To demonstrate the seasonal water storage effect on δ_{ET}, we first create a simple model experiment that is forced by contrasting wet and dry season water fluxes characteristic of inland Eurasia as shown in Figure 10. The *T*/*ET* is set to 60% for both seasons, an important assumption that is discussed later. Table 2 lists other relevant model inputs including the isotopic composition of precipitation as well as model results. In this experiment, we assume the initial water storage $S_0 = 200$ mm. In fact, the exact quantity of water storage from surface to subsurface is challenging to measure and observe. Güntner et al. (2007) provided a modeling perspective on the total water storage in different parts of the world. Based on their analysis, the mean annual water storage in continental climates that characterize Eurasia is about 260 mm with a seasonal amplitude of 160 mm, which justifies our choice of S_0. By extension, we note that the idealized water storage defined in our simple model refers to an isotopically homogenous, dynamic water storage that is refreshed by precipitation and removed by ET, and thus additionally includes deeper weathered bedrock moisture and groundwater reservoirs not considered by Güntner et al. (2007) (Rempe & Dietrich, 2018; Wang-Erlandsson et al., 2016).

Table 2
Model Inputs and Results for the Simple Model Experiment of the Seasonal Water Storage Model

	Wet season	Dry season
Water flux inputs		
Precipitation (mm)	350 (P_1)	210 (P_2)
Runoff (mm)	87.5 (R_1)	52.5 (R_2)
ET (mm)	140 (ET_1)	280 (ET_2)
Physical climate inputs		
Temperature (°C)	5	15
RH (%)	80	65
Aerodynamic exponent	0.8	0.8
Ecosystem condition inputs		
T/*ET*	0.6	0.6
Relative water storage size (S_0/P_1)	0.57	NA
Isotope flux inputs		
Precipitation $\delta^{18}O$ (‰)	−10	−6
Precipitation d-excess (‰)	10	10
Model results		
Modified source water $\delta^{18}O$ (‰)	−6.0 (δ_{I_1})	−4.9 (δ_{I_2})
ET $\delta^{18}O$ (‰)	−9.9 (δ_{ET_1})	−7.8 (δ_{ET_2})
Residual water storage $\delta^{18}O$ (‰)	−4.3 (δ_{S_1})	−0.8 (δ_{S_0} or δ_{S_2})
Modified source water d-excess (‰)	1.1	1.9
ET d-excess (‰)	8.4	10.8
Residual water storage d-excess (‰)	−2.1	−10.6

In Figure S4 in Supporting Information S1, we show that any given pair of δ_{P_1} and δ_{P_2} values will yield a unique suite of δ_{S_0}, δ_{S_1}, δ_{ET_1}, and δ_{ET_2} values if other model inputs are kept unchanged. These contour line plots demonstrate that δ_{ET_1} is primarily determined by δ_{P_1} (nearly vertical contours in Figure S4c in Supporting Information S1), whereas δ_{ET_2} reflects both δ_{P_2} as well as δ_{P_1} (not horizontal but somewhat sloping contours in Figure S4d in Supporting Information S1) due to the large wet season water storage that supplies the dry season ET. The strength of this δ_{P_1} memory effect is dependent on the amount of water storage relative to precipitation fluxes, encapsulated in our terms X_1 and X_2. Güntner et al. (2007) estimated that the ratio between the mean annual total water storage and precipitation amount, which we refer to as the storage-precipitation ratio hereafter, is about 0.2 at the global scale and is lower (0.1) in dry climates and higher (>0.35) in continental and polar/alpine climates. Besides the background climate effect examined by Güntner et al. (2007), the local water storage size and storage-precipitation ratio are shaped by many biotic and abiotic factors that vary widely across continents. For example, different bedrock types, by controlling the subsurface critical zone depth, lead to different water storage capacities and support different vegetation communities in the same region (Hahm et al., 2019). Some deep-rooted trees in arid climates tap bedrock moisture and groundwater, and

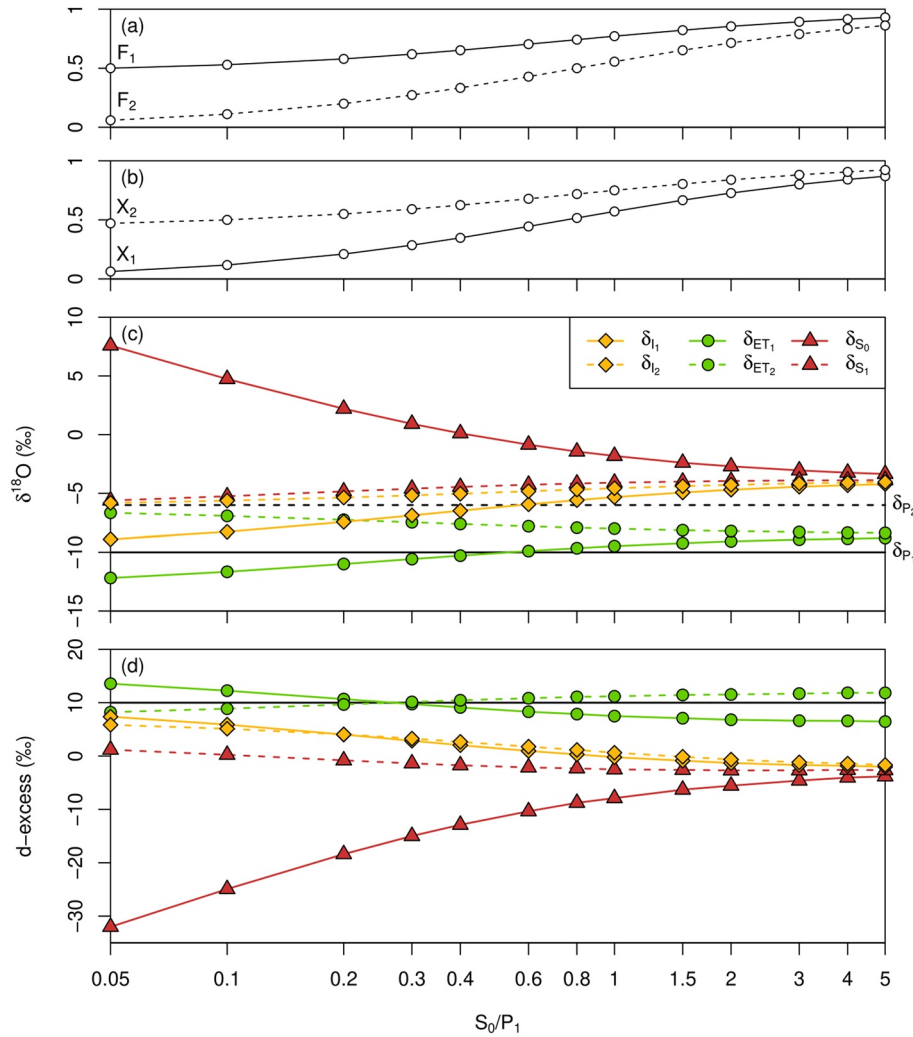

Figure 11. The summary of results from multiple seasonal water storage model experiments with variable S_0/P_1 values. (a) The fraction of residual liquid water remaining after evapotranspiration (ET) loss. (b) The fraction of residual water storage in the modified source water for ET. (c) The isotopic composition ($\delta^{18}O$) of precipitation, modified source water, ET, and residual water storage for the wet and dry seasons. (d) Similar to (c) but for d-excess.

as a result, may have access to large water storage underneath that are somewhat characteristic of humid climates (Fan et al., 2017; Scott et al., 2021).

To evaluate the sensitivity of model results to the relative size of water storage, we run multiple model experiments with variable initial water storage S_0 relative to P_1. The model script is provided as Data Set S2 and the results are summarized in Figure 11. As S_0/P_1 increases, δ_{S_0} and δ_{S_1} converge on the same value. Under this condition, the isotopic composition of water storage is static between wet and dry seasons as any precipitation and ET fluxes are too small (i.e., $X_1 \approx X_2 \approx 1$) to isotopically modify the existing large water storage reservoir. Further, with $\delta_{I_1} \approx \delta_{I_2}$ and $F_1 \approx F_2 \approx 1$, δ_{ET_1} and δ_{ET_2} are only dependent on physical climate conditions and T/ET according to Equation 15. As the d-excess of ET is very sensitive to surface RH (Aemisegger et al., 2014; Xia & Winnick, 2021), the lower RH in the dry season leads to a 5‰ higher d-excess of ET than in the wet season. Given that Güntner et al. (2007) determined a low global storage-precipitation ratio of only about 0.2, we consider that the very high S_0/P_1 condition is rare in nature and only represents certain rock moisture-dependent or groundwater-dependent ecosystems. By contrast, as S_0/P_1 decreases, F_2 decreases toward 0, meaning that the dry season ET removes nearly all available source water with $\delta_{ET_2} \approx \delta_{I_2}$. Under this condition, the dry season ET inherits the high $\delta^{18}O$ and low d-excess signal of the wet season water storage that contributes half of the source water ($X_2 \approx 0.5$). Conversely, the wet season ET has very little isotopic memory of the dry season water storage,

which is a very small fraction compared to the new precipitation input ($X_1 \approx 0$), even though the dry season water storage itself has even higher $\delta^{18}O$ and lower d-excess values. As a result of this seasonally varied water storage contribution, the d-excess of the wet season ET is about 5‰ higher than that of the dry season ET. We consider that the very low S_0/P_1 condition represents terrestrial ecosystems with shallow soils and limited hydrological connections with deeper water reservoirs, such as shallow-rooted grasslands.

These model experiments with variable S_0 indicate that the relative size of water storage directly controls the isotopic composition of ET fluxes. While we have assumed the same 10‰ d-excess in precipitation for both seasons, the d-excess of the dry season ET becomes lower than that of the wet season ET as the relative size of water storage decreases, and higher as the relative size of water storage increases; the transition occurs at about $S_0/P_1 = 0.3$. Most notably, the d-excess of ET fluxes may be lower than the d-excess of precipitation during the same season due to the contribution of residual water storage to the source water (Figure 11d). This challenges the simplistic view that moisture recycling progressively increases the d-excess signal in water vapor and precipitation along moisture transport pathways toward continental interiors (Gat & Matsui, 1991; Xia & Winnick, 2021). Instead, under particular water storage conditions, moisture recycling may act to decrease the d-excess in continental interiors on seasonal time scales. This is likely a widespread phenomenon in the dry season because the global storage-precipitation ratio is low (Güntner et al., 2007). Similar mechanisms have been invoked from direct isotopic measurements of ET fluxes in semiarid regions (Parkes et al., 2017) and the modeled isotopic composition of evaporation fluxes from a small, highly seasonal lake (Vallet-Coulomb et al., 2008). Our seasonal water storage model provides a simple framework that underscores the role of residual water storage in modulating the d-excess of ET fluxes and can be validated further by isotopic measurements of water vapor (Parkes et al., 2017; Ueta et al., 2014; Wei & Lee, 2019).

As mentioned earlier, in all these model experiments, we have assumed that the *T*/*ET* is 60% for both seasons. As an important simplification, this choice of transpiration fraction is an intermediate value among many reported *T*/*ET* values in the literature across sites and biomes and by a wide range of approaches (Fatichi & Pappas, 2017; Sutanto et al., 2014; Wei et al., 2017). That said, the partitioning of ET fluxes should vary seasonally driven by water availability and plant phenology. In addition to this first scenario of constant $T/ET = 60\%$, we consider two alternative scenarios. The second scenario is that the *T*/*ET* is 50% and 70% for the wet and dry seasons, respectively. This scenario is based on the empirical evidence that transpiration fraction in ET increases nonlinearly with leaf area index (Wang et al., 2014; Wei et al., 2017), which reaches peak values during the warm and often dry ($P < ET$) season when energy-driven plant water use is enhanced and surface evaporation is limited by water availability (Garrigues et al., 2008; Scott et al., 2021). The third scenario is the opposite in that the *T*/*ET* is 70% and 50% for the wet and dry seasons, respectively. This scenario represents some water-limited environments such as shallow-rooted grasslands where low water availability inhibits plant transpiration more than surface evaporation, leading to the relatively lower *T*/*ET* in the dry season (Cui et al., 2020; Scott et al., 2021). The tradeoff in water-energy fluxes and transition in ET partitioning have been previously shown in hydrological models (Maxwell & Condon, 2016).

The results of model experiments using alternative scenarios of *T*/*ET* partitioning are shown in Figure 12 by plotting the relative difference between the d-excess of the wet and dry season ET, hereafter referred to as the ET Δd-excess. In the second scenario where the transpiration fraction is higher in the dry season, the d-excess of the wet season ET is consistently higher than that of the dry season ET (ET Δd-excess > 0‰) even under high S_0/P_1 conditions. In the third scenario where the transpiration fraction is lower in the dry season, the result is the opposite (ET Δd-excess < 0‰ except when $S_0/P_1 = 0.05$). These suggest that the seasonal shift in ET partitioning controls the direction of ET Δd-excess. For both these alternative scenarios of *T*/*ET* partitioning, the effects of relative water storage size are still similar, with increasing ET Δd-excess (more positive) under decreasing S_0/P_1.

Finally, we interrogate the sensitivity and uncertainty of the above results to model inputs using an MC approach described in Text S1 in Supporting Information. The overall results shown in Figure S5 in Supporting Information S1 suggest that any slightly different choice of model inputs from Table 2 will lead to a considerable scattering in ET Δd-excess up to ±5‰ for the first *T*/*ET* partitioning scenario and up to ±8‰ for the second and third *T*/*ET* partitioning scenarios. However, the variability in model inputs does not change the pattern in the response of ET Δd-excess to S_0/P_1 and *T*/*ET*.

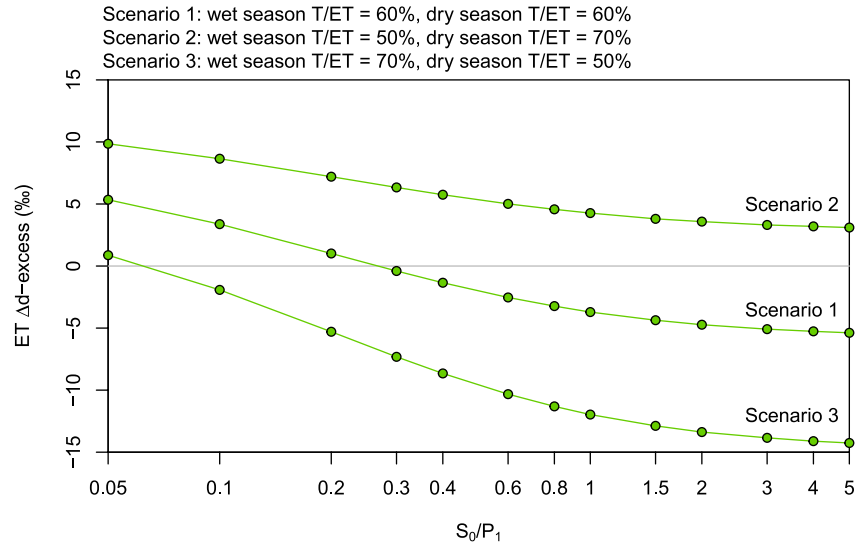

Figure 12. The relative difference between the d-excess of the wet and dry season evapotranspiration (ET Δd-excess) under variable S_0/P_1 and three ET partitioning scenarios.

6.3. Implications

The presented model for δ_{ET} based on simple mass balance demonstrates how the continental water storage and tradeoff in water use pathways modulate the d-excess of ET fluxes. As a result of these interactions in land surface ecohydrology, the d-excess of precipitation in continental interiors, which is substantially supplied by recycled moisture, is relatively insensitive to seasonal swings in the amount of recycled moisture on seasonal time scales. It does, however, have a complex response to regional-scale surface water balance and plant activity. This model framework explains the seasonal pattern of CV d-excess in Buenos Aires (Figure 2a): the highest CV d-excess occurs in MAM when the local and upwind terrestrial environments have an overall positive water balance unlike other seasons (Figure 7 and Movie S1). As a result, the lower contribution of residual water storage in MAM increases the d-excess of ET fluxes. Moreover, previous studies have found, as shown in Figure 6 as well, that the d-excess of precipitation is higher in autumn than in spring in Europe (Froehlich et al., 2008) such as Artern (Figure 3c), Siberia (Kurita et al., 2005), and central Asia (Pang et al., 2011), which were attributed to higher evaporation fractions in autumn. This is true for evaporation from large lakes (Corcoran et al., 2019), but site-level ET partitioning studies from these regions show higher ecosystem *T*/*ET* in autumn than in spring and thus disagree (e.g., Wang et al., 2014; Zhou et al., 2018). An alternative explanation is that the higher precipitation d-excess in autumn is caused by lower residual water storage contributions to ET fluxes, as shown by the widespread positive water balance conditions across Eurasia, in contrast to in spring (Figures 7b and 7d).

7. Conclusions and Implications

The d-excess of precipitation has been frequently explored in isotope hydrology and climatology literature, which often provide simplistic, qualitative interpretations of observed d-excess values and variations. However, d-excess values comprise complex information from oceanic evaporation conditions, subsequent distillations, moisture recycling, as well as local supersaturation conditions in vapor deposition, subcloud raindrop re-evaporation, and/or equilibration. All of these source-route-sink effects have been previously described; however, there is a lack of in-depth understanding of how these multiple processes compete or reinforce to produce the ultimate d-excess signals in continental precipitation that are measured. We present a new analysis in an attempt to unravel the mechanisms of seasonal variations in precipitation d-excess in non-polar regions. The key findings are the following:

1. The local condensation-induced shift between precipitation and vapor d-excess needs to be corrected to understand the d-excess seasonality in precipitation stations and to compare it with the d-excess of oceanic source

vapor. Raw precipitation and converted vapor d-excess may show different seasonal patterns due to this local overprinting.

2. Idealized Rayleigh distillation may lead to d-excess changes of ±3‰ or even more under certain initial conditions of vapor $\delta^{18}O$ and condensation temperature. This mechanism explains continental-scale spatial variations in d-excess in mid-latitude winters when there is a large oceanic distillation with ineffective moisture recycling and raindrop re-evaporation.
3. Raindrop re-evaporation, controlled by local RH, shows a dominant control on precipitation d-excess in low-latitudes and overprints the signal of oceanic evaporation conditions. This mechanism is, in part, associated with the effect of the convective activity responsible for the isotopic "amount effect."
4. Precipitation d-excess in mid-latitudes is primarily controlled by the seasonal changes in oceanic evaporation conditions. However, there are also large, concurrent changes in the effects of raindrop re-evaporation and moisture recycling that contribute to modulating the seasonality in d-excess. Developing strategies to quantify and separate these individual effects should be the focus of future studies.
5. Although presumably moisture recycling may result in increasing d-excess in water vapor and precipitation toward continental interiors, we find little evidence for these dynamics on seasonal time scales when large swings in moisture recycling occur. We use a simple seasonal water storage model to demonstrate that the d-excess of ET fluxes is controlled by the size of water storage and partitioning between evaporation and transpiration. As a result, the dry season ET may counter-intuitively have lower d-excess due to the contribution of residual water storage to ET fluxes and higher transpiration fractions, than the dry season precipitation and wet season ET, despite enhanced continental moisture recycling.

Taken together, this study combines global data analysis and a hierarchy of parsimonious models to raise awareness that the d-excess in precipitation is a complex parameter controlled by multiple processes and that nonconservative behavior in d-excess is ubiquitous throughout the water cycle. Therefore, the fidelity of d-excess as a tracer for remote conditions at oceanic moisture sources should be critically appraised. These caveats need to be considered in future hydrological or paleoclimate investigations wherever precipitation (or more generally, meteoric water) d-excess data are used.

We introduce a few cutting-edge techniques that may play a key role in advancing the research agenda. First, specialized instrumentations such as in situ or satellite isotopic measurements of water vapor may assist in disentangling these complex dynamics in d-excess (Aemisegger et al., 2014; Akers et al., 2020; Bastrikov et al., 2014; Graf et al., 2019; Worden et al., 2007). It is worth noting that water vapor measurements are transient in nature and many data are not directly related to precipitation events (Frankenberg et al., 2009). Second, the currently growing database of novel precipitation $\Delta'^{17}O$ measurements provides a new lens for tracking kinetic fractionations in the water cycle (Aron et al., 2021; Landais et al., 2010; Li et al., 2015; Luz & Barkan, 2010), but there is a lack of research investigating how to leverage the paired d-excess and $\Delta'^{17}O$ data for fingerprinting water cycle processes. Finally, isotope-enabled GCMs are powerful, albeit expensive, tools to investigate the isotopic variability of precipitation and water vapor during instrumental periods and in past climates (Schoenemann et al., 2014; Steen-Larsen et al., 2017; Vuille et al., 2003). The isotope-enabled GCMs do have the potential to tease apart the respective contribution of multiple processes to the variability in d-excess, as shown in a few previous studies (Jouzel et al., 2013; Lewis et al., 2013; Risi et al., 2013). This study also means that an accurate representation of d-excess values and seasonal variations is desired for the future development and calibration of isotope-enabled GCMs.

Data Availability Statement

The USNIP program data (spanning 1989–2001) used in this study, including raw weekly data ($\delta^{18}O$ and d-excess) and 12-monthly means for each station (both RP and CV values), are provided in Data Set S1. Because JMW has dedicated decades to collecting and compiling this data set for the benefit of the community, collaborative data use in future research projects with JMW would be appropriate; especially those whereby a publishable product, manuscript, maps, or visualizations are not possible without the use and application of this data set. The R script for running the seasonal water storage model with variable water storage sizes is provided in Data Set S2. Additionally, the GNIP program data (IAEA/WMO, 2021) can be accessed from https://www.iaea.org/services/networks/gnip. The ERA5 reanalysis data (C3S, 2021) can be accessed from https://www.ecmwf.int/en/forecasts/datasets/reanalysis-datasets/era5.

Acknowledgments
This work was supported by the UMass Faculty Startup Fund to MJW. ZX was supported in part by the Fundamental Research Funds for the Central Universities (135112004). The USNIP program has been funded by the NSF awards (9413903, 9871262, 0923571) to JMW. JMW was supported in part by the UArctic Research Chairship. We thank two reviewers whose comments and suggestions improved earlier versions of this manuscript, Angela Ampuero Grández, Andreas Link, and Ruud van der Ent for suggestions on the WAM-2layers.

References

Aemisegger, F., Pfahl, S., Sodemann, H., Lehner, I., Seneviratne, S. I., & Wernli, H. (2014). Deuterium excess as a proxy for continental moisture recycling and plant transpiration. *Atmospheric Chemistry and Physics*, *14*(8), 4029–4054. https://doi.org/10.5194/acp-14-4029-2014

Aggarwal, P. K., Alduchov, O. A., Froehlich, K. O., Araguas-Araguas, L. J., Sturchio, N. C., & Kurita, N. (2012). Stable isotopes in global precipitation: A unified interpretation based on atmospheric moisture residence time. *Geophysical Research Letters*, *39*, L11705. https://doi.org/10.1029/2012GL051937

Akers, P. D., Kopec, B. G., Mattingly, K. S., Klein, E. S., Causey, D., & Welker, J. M. (2020). Baffin Bay sea ice extent and synoptic moisture transport drive water vapor isotope ($\delta^{18}O$, $\delta^{2}H$, and deuterium excess) variability in coastal northwest Greenland. *Atmospheric Chemistry and Physics*, *20*(22), 13929–13955. https://doi.org/10.5194/acp-20-13929-2020

Ampuero, A., Stríkis, N. M., Apaéstegui, J., Vuille, M., Novello, V. F., Espinoza, J. C., et al. (2020). The forest effects on the isotopic composition of rainfall in the northwestern Amazon basin. *Journal of Geophysical Research: Atmospheres*, *125*, e2019JD031445. https://doi.org/10.1029/2019JD031445

Angert, A., Cappa, C. D., & DePaolo, D. J. (2004). Kinetic ^{17}O effects in the hydrologic cycle: Indirect evidence and implications. *Geochimica et Cosmochimica Acta*, *68*(17), 3487–3495. https://doi.org/10.1016/j.gca.2004.02.010

Araguás-Araguás, L., Froehlich, K., & Rozanski, K. (1998). Stable isotope composition of precipitation over southeast Asia. *Journal of Geophysical Research*, *103*(D22), 28721–28742. https://doi.org/10.1029/98JD02582

Aron, P. G., Levin, N. E., Beverly, E. J., Huth, T. E., Passey, B. H., Pelletier, E. M., et al. (2021). Triple oxygen isotopes in the water cycle. *Chemical Geology*, *565*, 120026. https://doi.org/10.1016/j.chemgeo.2020.120026

Bailey, A., Posmentier, E., & Feng, X. (2018). Patterns of evaporation and precipitation drive global isotopic changes in atmospheric moisture. *Geophysical Research Letters*, *45*, 7093–7101. https://doi.org/10.1029/2018GL078254

Bastrikov, V., Steen-Larsen, H. C., Masson-Delmotte, V., Gribanov, K., Cattani, O., Jouzel, J., & Zakharov, V. (2014). Continuous measurements of atmospheric water vapour isotopes in western Siberia (Kourovka). *Atmospheric Measurement Techniques*, *7*(6), 1763–1776. https://doi.org/10.5194/amt-7-1763-2014

Benetti, M., Reverdin, G., Pierre, C., Merlivat, L., Risi, C., Steen-Larsen, H. C., & Vimeux, F. (2014). Deuterium excess in marine water vapor: Dependency on relative humidity and surface wind speed during evaporation. *Journal of Geophysical Research: Atmospheres*, *119*, 584–593. https://doi.org/10.1002/2013JD020535

Birks, S. J., & Gibson, J. J. (2009). Isotope hydrology research in Canada, 2003–2007. *Canadian Water Resources Journal*, *34*(2), 163–176. https://doi.org/10.4296/cwrj3402163

Bolton, D. (1980). The computation of equivalent potential temperature. *Monthly Weather Review*, *108*(7), 1046–1053. https://doi.org/10.1175/1520-0493(1980)108<1046:TCOEPT>2.0.CO;2

Bonne, J. L., Meyer, H., Behrens, M., Boike, J., Kipfstuhl, S., Rabe, B., et al. (2020). Moisture origin as a driver of temporal variabilities of the water vapour isotopic composition in the Lena River Delta, Siberia. *Atmospheric Chemistry and Physics*, *20*(17), 10493–10511. https://doi.org/10.5194/acp-20-10493-2020

Bony, S., Risi, C., & Vimeux, F. (2008). Influence of convective processes on the isotopic composition ($\delta^{18}O$ and δD) of precipitation and water vapor in the tropics: 1. Radiative-convective equilibrium and Tropical Ocean-Global Atmosphere-Coupled Ocean-Atmosphere Response Experiment (TOGA-COARE) simulations. *Journal of Geophysical Research*, *113*, D19305. https://doi.org/10.1029/2008JD009942

Bowen, G. J. (2008). Spatial analysis of the intra-annual variation of precipitation isotope ratios and its climatological corollaries. *Journal of Geophysical Research*, *113*, D05113. https://doi.org/10.1029/2007JD009295

Bowen, G. J. (2010). Isoscapes: Spatial pattern in isotopic biogeochemistry. *Annual Review of Earth and Planetary Sciences*, *38*, 161–187. https://doi.org/10.1146/annurev-earth-040809-152429

Bowen, G. J., Cai, Z., Fiorella, R. P., & Putman, A. L. (2019). Isotopes in the water cycle: Regional- to global-scale patterns and applications. *Annual Review of Earth and Planetary Sciences*, *47*(1), 453–479. https://doi.org/10.1146/annurev-earth-053018-060220

Bowen, G. J., Wassenaar, L. I., & Hobson, K. A. (2005). Global application of stable hydrogen and oxygen isotopes to wildlife forensics. *Oecologia*, *143*(3), 337–348. https://doi.org/10.1007/s00442-004-1813-y

C3S. (2021). ERA5: Fifth generation of ECMWF atmospheric reanalyses of the global climate. [Dataset]. Copernicus Climate Change Service Climate Data Store (CDS). Retrieved from https://www.ecmwf.int/en/forecasts/datasets/reanalysis-datasets/era5

Cai, Z., & Tian, L. (2016). Atmospheric controls on seasonal and interannual variations in the precipitation isotope in the East Asian monsoon region. *Journal of Climate*, *29*(4), 1339–1352. https://doi.org/10.1175/JCLI-D-15-0363.1

Cai, Z., Tian, L., & Bowen, G. J. (2018). Spatial-seasonal patterns reveal large-scale atmospheric controls on Asian Monsoon precipitation water isotope ratios. *Earth and Planetary Science Letters*, *503*, 158–169. https://doi.org/10.1016/j.epsl.2018.09.028

Ciais, P., & Jouzel, J. (1994). Deuterium and oxygen 18 in precipitation: Isotopic model, including mixed cloud processes. *Journal of Geophysical Research*, *99*(D8), 16793–16803. https://doi.org/10.1029/94JD00412

Cluett, A. A., Thomas, E. K., Evans, S. M., & Keys, P. W. (2021). Seasonal variations in moisture origin explain spatial contrast in precipitation isotope seasonality on coastal western Greenland. *Journal of Geophysical Research: Atmospheres*, *126*, e2020JD033543. https://doi.org/10.1029/2020JD033543

Conroy, J. L., Noone, D., Cobb, K. M., Moerman, J. W., & Konecky, B. L. (2016). Paired stable isotopologues in precipitation and vapor: A case study of the amount effect within western tropical Pacific storms. *Journal of Geophysical Research: Atmospheres*, *121*, 3290–3303. https://doi.org/10.1002/2015JD023844

Corcoran, M. C., Thomas, E. K., & Boutt, D. F. (2019). Event-based precipitation isotopes in the Laurentian Great Lakes region reveal spatiotemporal patterns in moisture recycling. *Journal of Geophysical Research: Atmospheres*, *124*, 5463–5478. https://doi.org/10.1029/2018JD029545

Craig, H. (1961). Isotopic variations in meteoric waters. *Science*, *133*(3465), 1702–1703. https://doi.org/10.1126/science.133.3465.1702

Craig, H., & Gordon, L. I. (1965). Deuterium and oxygen 18 variations in the ocean and the marine atmosphere. In E. Tongiorgi (Ed.), *Proceedings of a Conference on Stable Isotopes in Oceanographic Studies and Paleotemperatures, Spoleto, Italy* (pp. 9–130).

Crawford, J., Hollins, S. E., Meredith, K. T., & Hughes, C. E. (2017). Precipitation stable isotope variability and subcloud evaporation processes in a semi-arid region. *Hydrological Processes*, *31*(1), 20–34. https://doi.org/10.1002/hyp.10885

Cui, J., Tian, L., Wei, Z., Huntingford, C., Wang, P., Cai, Z., et al. (2020). Quantifying the controls on evapotranspiration partitioning in the highest alpine meadow ecosystem. *Water Resources Research*, *56*, e2019WR024815. https://doi.org/10.1029/2019WR024815

Dansgaard, W. (1964). Stable isotopes in precipitation. *Tellus*, *16*(4), 436–468. https://doi.org/10.3402/tellusa.v16i4.8993

Dee, D. P., Uppala, S. M., Simmons, A. J., Berrisford, P., Poli, P., Kobayashi, S., et al. (2011). The ERA-Interim reanalysis: Configuration and performance of the data assimilation system. *Quarterly Journal of the Royal Meteorological Society*, *137*(656), 553–597. https://doi.org/10.1002/qj.828

Dee, S., Noone, D., Buenning, N., Emile-Geay, J., & Zhou, Y. (2015). SPEEDY-IER: A fast atmospheric GCM with water isotope physics. *Journal of Geophysical Research: Atmospheres*, *120*, 73–91. https://doi.org/10.1002/2014JD022194

Delmotte, M., Masson, V., Jouzel, J., & Morgan, V. I. (2000). A seasonal deuterium excess signal at Law Dome, coastal eastern Antarctica: A Southern Ocean signature. *Journal of Geophysical Research*, *105*(D6), 7187–7197. https://doi.org/10.1029/1999JD901085

Dongmann, G., Nürnberg, H. W., Förstel, H., & Wagener, K. (1974). On the enrichment of $H_2{}^{18}O$ in the leaves of transpiring plants. *Radiation and Environmental Biophysics*, *11*(1), 41–52. https://doi.org/10.1007/BF01323099

Dütsch, M., Blossey, P. N., Steig, E. J., & Nusbaumer, J. M. (2019). Nonequilibrium fractionation during ice cloud formation in iCAM5: Evaluating the common parameterization of supersaturation as a linear function of temperature. *Journal of Advances in Modeling Earth Systems*, *11*(11), 3777–3793. https://doi.org/10.1029/2019MS001764

Dütsch, M., Pfahl, S., & Sodemann, H. (2017). The impact of nonequilibrium and equilibrium fractionation on two different deuterium excess definitions. *Journal of Geophysical Research: Atmospheres*, *122*, 12732–12746. https://doi.org/10.1002/2017JD027085

Eltahir, E. A. B., & Bras, R. L. (1994). Precipitation recycling in the Amazon basin. *Quarterly Journal of the Royal Meteorological Society*, *120*(518), 861–880. https://doi.org/10.1002/qj.49712051806

Fan, Y., Miguez-Macho, G., Jobbágy, E. G., Jackson, R. B., & Otero-Casal, C. (2017). Hydrologic regulation of plant rooting depth. *Proceedings of the National Academy of Sciences of the United States of America*, *114*(40), 10572–10577. https://doi.org/10.1073/pnas.1712381114

Fatichi, S., & Pappas, C. (2017). Constrained variability of modeled *T:ET* ratio across biomes. *Geophysical Research Letters*, *44*, 6795–6803. https://doi.org/10.1002/2017GL074041

Feng, X., Faiia, A. M., & Posmentier, E. S. (2009). Seasonality of isotopes in precipitation: A global perspective. *Journal of Geophysical Research*, *114*, D08116. https://doi.org/10.1029/2008JD011279

Flanagan, L. B., Comstock, J. P., & Ehleringer, J. R. (1991). Comparison of modeled and observed environmental influences on the stable oxygen and hydrogen isotope composition of leaf water in *Phaseolus vulgaris* L. *Plant Physiology*, *96*(2), 588–596. https://doi.org/10.1104/pp.96.2.588

Frankenberg, C., Yoshimura, K., Warneke, T., Aben, I., Butz, A., Deutscher, N., et al. (2009). Dynamic processes governing lower-tropospheric HDO/H_2O ratios as observed from space and ground. *Science*, *325*(5946), 1374–1377. https://doi.org/10.1126/science.1173791

Froehlich, K., Gibson, J. J., & Aggarwal, P. K. (2002). Deuterium excess in precipitation and its climatological significance (IAEA-CSP-13/P). *International Atomic Energy Agency (IAEA)*. Retrieved from https://inis.iaea.org/search/search.aspx?orig_q=RN:34017972

Froehlich, K., Kralik, M., Papesch, W., Rank, D., Scheifinger, H., & Stichler, W. (2008). Deuterium excess in precipitation of Alpine regions—Moisture recycling. *Isotopes in Environmental and Health Studies*, *44*(1), 61–70. https://doi.org/10.1080/10256010801887208

Garrigues, S., Lacaze, R., Baret, F., Morisette, J. T., Weiss, M., Nickeson, J. E., et al. (2008). Validation and intercomparison of global Leaf Area Index products derived from remote sensing data. *Journal of Geophysical Research*, *113*, G02028. https://doi.org/10.1029/2007JG000635

Gat, J. R. (1996). Oxygen and hydrogen isotopes in the hydrological cycle. *Annual Review of Earth and Planetary Sciences*, *24*, 225–262. https://doi.org/10.1146/annurev.earth.24.1.225

Gat, J. R., & Airey, P. L. (2006). Stable water isotopes in the atmosphere/biosphere/lithosphere interface: Scaling-up from the local to continental scale, under humid and dry conditions. *Global and Planetary Change*, *51*(1), 25–33. https://doi.org/10.1016/j.gloplacha.2005.12.004

Gat, J. R., Bowser, C. J., & Kendall, C. (1994). The contribution of evaporation from the Great Lakes to the continental atmosphere: Estimate based on stable isotope data. *Geophysical Research Letters*, *21*(7), 557–560. https://doi.org/10.1029/94GL00069

Gat, J. R., & Matsui, E. (1991). Atmospheric water balance in the Amazon basin: An isotopic evapotranspiration model. *Journal of Geophysical Research*, *96*(D7), 13179–13188. https://doi.org/10.1029/91JD00054

Gimeno, L., Drumond, A., Nieto, R., Trigo, R. M., & Stohl, A. (2010). On the origin of continental precipitation. *Geophysical Research Letters*, *37*, L13804. https://doi.org/10.1029/2010GL043712

Graf, P., Wernli, H., Pfahl, S., & Sodemann, H. (2019). A new interpretative framework for below-cloud effects on stable water isotopes in vapour and rain. *Atmospheric Chemistry and Physics*, *19*(2), 747–765. https://doi.org/10.5194/acp-19-747-2019

Guan, H., Zhang, X., Skrzypek, G., Sun, Z., & Xu, X. (2013). Deuterium excess variations of rainfall events in a coastal area of South Australia and its relationship with synoptic weather systems and atmospheric moisture sources. *Journal of Geophysical Research: Atmospheres*, *118*, 1123–1138. https://doi.org/10.1002/jgrd.50137

Güntner, A., Stuck, J., Werth, S., Döll, P., Verzano, K., & Merz, B. (2007). A global analysis of temporal and spatial variations in continental water storage. *Water Resources Research*, *43*, W05416. https://doi.org/10.1029/2006WR005247

Haese, B., Werner, M., & Lohmann, G. (2013). Stable water isotopes in the coupled atmosphere-land surface model ECHAM5-JSBACH. *Geoscientific Model Development*, *6*(5), 1463–1480. https://doi.org/10.5194/gmd-6-1463-2013

Hahm, W. J., Rempe, D. M., Dralle, D. N., Dawson, T. E., Lovill, S. M., Bryk, A. B., et al. (2019). Lithologically controlled subsurface critical zone thickness and water storage capacity determine regional plant community composition. *Water Resources Research*, *55*, 3028–3055. https://doi.org/10.1029/2018WR023760

Henderson-Sellers, A., Fischer, M., Aleinov, I., McGuffie, K., Riley, W. J., Schmidt, G. A., et al. (2006). Stable water isotope simulation by current land-surface schemes: Results of iPILPS Phase 1. *Global and Planetary Change*, *51*(1), 34–58. https://doi.org/10.1016/j.gloplacha.2006.01.003

Hendricks, M. B., DePaolo, D. J., & Cohen, R. C. (2000). Space and time variation of $\delta^{18}O$ and δD in precipitation: Can paleotemperature be estimated from ice cores? *Global Biogeochemical Cycles*, *14*(3), 851–861. https://doi.org/10.1029/1999GB001198

Hersbach, H., Bell, B., Berrisford, P., Hirahara, S., Horányi, A., Muñoz-Sabater, J., et al. (2020). The ERA5 global reanalysis. *Quarterly Journal of the Royal Meteorological Society*, *146*(730), 1999–2049. https://doi.org/10.1002/qj.3803

Hurrell, J. W., & Deser, C. (2010). North Atlantic climate variability: The role of the North Atlantic Oscillation. *Journal of Marine Systems*, *79*(3), 231–244. https://doi.org/10.1016/j.jmarsys.2009.11.002

IAEA/WMO. (2021). Global Network of Isotopes in Precipitation: The GNIP database [Dataset]. WISER Portal. Retrieved from https://www.iaea.org/services/networks/gnip

Jasechko, S., Sharp, Z. D., Gibson, J. J., Birks, S. J., Yi, Y., & Fawcett, P. J. (2013). Terrestrial water fluxes dominated by transpiration. *Nature*, *496*(7445), 347–350. https://doi.org/10.1038/nature11983

Johnsen, S. J., Dansgaard, W., & White, J. W. C. (1989). The origin of Arctic precipitation under present and glacial conditions. *Tellus B: Chemical and Physical Meteorology*, *41*(4), 452–468. https://doi.org/10.3402/tellusb.v41i4.15100

Jouzel, J., Delaygue, G., Landais, A., Masson-Delmotte, V., Risi, C., & Vimeux, F. (2013). Water isotopes as tools to document oceanic sources of precipitation. *Water Resources Research*, *49*, 7469–7486. https://doi.org/10.1002/2013WR013508

Jouzel, J., & Koster, R. D. (1996). A reconsideration of the initial conditions used for stable water isotope models. *Journal of Geophysical Research*, *101*(D17), 22933–22938. https://doi.org/10.1029/96JD02362

Jouzel, J., & Merlivat, L. (1984). Deuterium and oxygen 18 in precipitation: Modeling of the isotopic effects during snow formation. *Journal of Geophysical Research*, *89*(D7), 11749–11757. https://doi.org/10.1029/JD089iD07p11749

Jouzel, J., Merlivat, L., & Lorius, C. (1982). Deuterium excess in an East Antarctic ice core suggests higher relative humidity at the oceanic surface during the last glacial maximum. *Nature*, *299*(5885), 688–691. https://doi.org/10.1038/299688a0

Kaseke, K. F., Wang, L., Wanke, H., Tian, C., Lanning, M., & Jiao, W. (2018). Precipitation origins and key drivers of precipitation isotope (^{18}O, ^{2}H, and ^{17}O) compositions over Windhoek. *Journal of Geophysical Research: Atmospheres*, *123*, 7311–7330. https://doi.org/10.1029/2018JD028470

Keys, P. W., van der Ent, R. J., Gordon, L. J., Hoff, H., Nikoli, R., & Savenije, H. H. G. (2012). Analyzing precipitationsheds to understand the vulnerability of rainfall dependent regions. *Biogeosciences*, *9*(2), 733–746. https://doi.org/10.5194/bg-9-733-2012

Klein, E. S., Nolan, M., McConnell, J., Sigl, M., Cherry, J., Young, J., & Welker, J. M. (2016). McCall Glacier record of Arctic climate change: Interpreting a northern Alaska ice core with regional water isotopes. *Quaternary Science Reviews*, *131*, 274–284. https://doi.org/10.1016/j.quascirev.2015.07.030

Klein, E. S., & Welker, J. M. (2016). Influence of sea ice on ocean water vapor isotopes and Greenland ice core records. *Geophysical Research Letters*, *43*, 12475–12483. https://doi.org/10.1002/2016GL071748

Konecky, B. L., Noone, D. C., & Cobb, K. M. (2019). The influence of competing hydroclimate processes on stable isotope ratios in tropical rainfall. *Geophysical Research Letters*, *46*, 1622–1633. https://doi.org/10.1029/2018GL080188

Kong, Y., Pang, Z., & Froehlich, K. (2013). Quantifying recycled moisture fraction in precipitation of an arid region using deuterium excess. *Tellus B: Chemical and Physical Meteorology*, *65*(1), 19251. https://doi.org/10.3402/tellusb.v65i0.19251

Kopec, B. G., Feng, X., Michel, F. A., & Posmentier, E. S. (2016). Influence of sea ice on Arctic precipitation. *Proceedings of the National Academy of Sciences of the United States of America*, *113*(1), 46–51. https://doi.org/10.1073/pnas.1504633113

Kurita, N., Noone, D., Risi, C., Schmidt, G. A., Yamada, H., & Yoneyama, K. (2011). Intraseasonal isotopic variation associated with the Madden-Julian Oscillation. *Journal of Geophysical Research*, *116*, D24101. https://doi.org/10.1029/2010JD015209

Kurita, N., Sugimoto, A., Fujii, Y., Fukazawa, T., Makarov, V. N., Watanabe, O., et al. (2005). Isotopic composition and origin of snow over Siberia. *Journal of Geophysical Research*, *110*, D13102. https://doi.org/10.1029/2004JD005053

Kurita, N., & Yamada, H. (2008). The role of local moisture recycling evaluated using stable isotope data from over the middle of the Tibetan Plateau during the monsoon season. *Journal of Hydrometeorology*, *9*(4), 760–775. https://doi.org/10.1175/2007JHM945.1

Lamb, K. D., Clouser, B. W., Bolot, M., Sarkozy, L., Ebert, V., Saathoff, H., et al. (2017). Laboratory measurements of HDO/H_2O isotopic fractionation during ice deposition in simulated cirrus clouds. *Proceedings of the National Academy of Sciences of the United States of America*, *114*(22), 5612–5617. https://doi.org/10.1073/pnas.1618374114

Landais, A., Barkan, E., & Luz, B. (2008). Record of $\delta^{18}O$ and ^{17}O-excess in ice from Vostok Antarctica during the last 150,000 years. *Geophysical Research Letters*, *35*, L02709. https://doi.org/10.1029/2007GL032096

Landais, A., Risi, C., Bony, S., Vimeux, F., Descroix, L., Falourd, S., & Bouygues, A. (2010). Combined measurements of $^{17}O_{excess}$ and d-excess in African monsoon precipitation: Implications for evaluating convective parameterizations. *Earth and Planetary Science Letters*, *298*(1), 104–112. https://doi.org/10.1016/j.epsl.2010.07.033

Landais, A., Stenni, B., Masson-Delmotte, V., Jouzel, J., Cauquoin, A., Fourré, E., et al. (2021). Interglacial Antarctic-Southern Ocean climate decoupling due to moisture source area shifts. *Nature Geoscience*, *14*(12), 918–923. https://doi.org/10.1038/s41561-021-00856-4

Lee, J.-E., Fung, I., DePaolo, D. J., & Henning, C. C. (2007). Analysis of the global distribution of water isotopes using the NCAR atmospheric general circulation model. *Journal of Geophysical Research*, *112*, D16306. https://doi.org/10.1029/2006JD007657

Lewis, S. C., LeGrande, A. N., Kelley, M., & Schmidt, G. A. (2013). Modeling insights into deuterium excess as an indicator of water vapor source conditions. *Journal of Geophysical Research: Atmospheres*, *118*, 243–262. https://doi.org/10.1029/2012JD017804

Li, G., Hartmann, J., Derry, L. A., West, A. J., You, C.-F., Long, X., et al. (2016). Temperature dependence of basalt weathering. *Earth and Planetary Science Letters*, *443*, 59–69. https://doi.org/10.1016/j.epsl.2016.03.015

Li, S., Levin, N. E., & Chesson, L. A. (2015). Continental scale variation in ^{17}O-excess of meteoric waters in the United States. *Geochimica et Cosmochimica Acta*, *164*, 110–126. https://doi.org/10.1016/j.gca.2015.04.047

Liebminger, A., Haberhauer, G., Papesch, W., & Heiss, G. (2006). Correlation of the isotopic composition in precipitation with local conditions in alpine regions. *Journal of Geophysical Research*, *111*, D05104. https://doi.org/10.1029/2005JD006258

Lisi, P. J., Schindler, D. E., Cline, T. J., Scheuerell, M. D., & Walsh, P. B. (2015). Watershed geomorphology and snowmelt control stream thermal sensitivity to air temperature. *Geophysical Research Letters*, *42*, 3380–3388. https://doi.org/10.1002/2015GL064083

Liu, Z., Bowen, G. J., & Welker, J. M. (2010). Atmospheric circulation is reflected in precipitation isotope gradients over the conterminous United States. *Journal of Geophysical Research*, *115*, D22120. https://doi.org/10.1029/2010JD014175

Luz, B., & Barkan, E. (2010). Variations of $^{17}O/^{16}O$ and $^{18}O/^{16}O$ in meteoric waters. *Geochimica et Cosmochimica Acta*, *74*(22), 6276–6286. https://doi.org/10.1016/j.gca.2010.08.016

Majoube, M. (1971a). Fractionnement en oxygène 18 entre la glace et la vapeur d'eau. *Journal de Chimie Physique*, *68*, 625–636. https://doi.org/10.1051/jcp/1971680625

Majoube, M. (1971b). Fractionnement en oxygène 18 et deutérium entre l'eau et sa vapeur. *Journal de Chimie Physique*, *68*, 1423–1436. https://doi.org/10.1051/jcp/1971681423

Markle, B. R., Steig, E. J., Buizert, C., Schoenemann, S. W., Bitz, C. M., Fudge, T. J., et al. (2017). Global atmospheric teleconnections during Dansgaard-Oeschger events. *Nature Geoscience*, *10*(1), 36–40. https://doi.org/10.1038/ngeo2848

Martens, B., Miralles, D. G., Lievens, H., van der Schalie, R., de Jeu, R. A. M., Fernández-Prieto, D., et al. (2017). GLEAM v3: Satellite-based land evaporation and root-zone soil moisture. *Geoscientific Model Development*, *10*(5), 1903–1925. https://doi.org/10.5194/gmd-10-1903-2017

Masson-Delmotte, V., Jouzel, J., Landais, A., Stievenard, M., Johnsen, S. J., White, J. W. C., et al. (2005). GRIP deuterium excess reveals rapid and orbital-scale changes in Greenland moisture origin. *Science*, *309*(5731), 118–121. https://doi.org/10.1126/science.1108575

Maxwell, R. M., & Condon, L. E. (2016). Connections between groundwater flow and transpiration partitioning. *Science*, *353*(6297), 377–380. https://doi.org/10.1126/science.aaf7891

Merlivat, L. (1978). Molecular diffusivities of $H_2{}^{16}O$, $HD^{16}O$, and $H_2{}^{18}O$ in gases. *The Journal of Chemical Physics*, *69*(6), 2864–2871. https://doi.org/10.1063/1.436884

Merlivat, L., & Jouzel, J. (1979). Global climatic interpretation of the deuterium-oxygen 18 relationship for precipitation. *Journal of Geophysical Research*, *84*(C8), 5029–5033. https://doi.org/10.1029/JC084iC08p05029

Merlivat, L., & Nief, G. (1967). Fractionnement isotopique lors des changements d'état solide-vapeur et liquide-vapeur de l'eau à des températures inférieures à 0°C. *Tellus*, *19*(1), 122–127. https://doi.org/10.1111/j.2153-3490.1967.tb01465.x

Mix, H. T., Winnick, M. J., Mulch, A., & Page Chamberlain, C. (2013). Grassland expansion as an instrument of hydrologic change in Neogene western North America. *Earth and Planetary Science Letters*, *377–378*, 73–83. https://doi.org/10.1016/j.epsl.2013.07.032

Pang, Z., Kong, Y., Froehlich, K., Huang, T., Yuan, L., Li, Z., & Wang, F. (2011). Processes affecting isotopes in precipitation of an arid region. *Tellus B: Chemical and Physical Meteorology*, *63*(3), 352–359. https://doi.org/10.1111/j.1600-0889.2011.00532.x

Parkes, S. D., McCabe, M. F., Griffiths, A. D., Wang, L., Chambers, S., Ershadi, A., et al. (2017). Response of water vapour D-excess to land-atmosphere interactions in a semi-arid environment. *Hydrology and Earth System Sciences*, *21*(1), 533–548. https://doi.org/10.5194/hess-21-533-2017

Penna, D., Engel, M., Mao, L., Dell'Agnese, A., Bertoldi, G., & Comiti, F. (2014). Tracer-based analysis of spatial and temporal variations of water sources in a glacierized catchment. *Hydrology and Earth System Sciences*, *18*(12), 5271–5288. https://doi.org/10.5194/hess-18-5271-2014

Petit, J. R., White, J. W. C., Young, N. W., Jouzel, J., & Korotkevich, Y. S. (1991). Deuterium excess in recent Antarctic snow. *Journal of Geophysical Research*, *96*(D3), 5113–5122. https://doi.org/10.1029/90JD02232

Pfahl, S., & Sodemann, H. (2014). What controls deuterium excess in global precipitation? *Climate of the Past*, *10*(2), 771–781. https://doi.org/10.5194/cp-10-771-2014

Pfahl, S., & Wernli, H. (2008). Air parcel trajectory analysis of stable isotopes in water vapor in the eastern Mediterranean. *Journal of Geophysical Research*, *113*, D20104. https://doi.org/10.1029/2008JD009839

Pfahl, S., & Wernli, H. (2009). Lagrangian simulations of stable isotopes in water vapor: An evaluation of nonequilibrium fractionation in the Craig-Gordon model. *Journal of Geophysical Research*, *114*, D20108. https://doi.org/10.1029/2009JD012054

Putman, A. L., Bowen, G. J., & Strong, C. (2021). Local and regional modes of hydroclimatic change expressed in modern multidecadal precipitation oxygen isotope trends. *Geophysical Research Letters*, *48*, e2020GL092006. https://doi.org/10.1029/2020GL092006

Putman, A. L., Fiorella, R. P., Bowen, G. J., & Cai, Z. (2019). A global perspective on Local Meteoric Water Lines: Meta-analytic insight into fundamental controls and practical constraints. *Water Resources Research*, *55*, 6896–6910. https://doi.org/10.1029/2019WR025181

Rempe, D. M., & Dietrich, W. E. (2018). Direct observations of rock moisture, a hidden component of the hydrologic cycle. *Proceedings of the National Academy of Sciences of the United States of America*, *115*(11), 2664–2669. https://doi.org/10.1073/pnas.1800141115

Risi, C., Bony, S., & Vimeux, F. (2008). Influence of convective processes on the isotopic composition ($\delta^{18}O$ and δD) of precipitation and water vapor in the tropics: 2. Physical interpretation of the amount effect. *Journal of Geophysical Research*, *113*, D19306. https://doi.org/10.1029/2008JD009943

Risi, C., Bony, S., Vimeux, F., & Jouzel, J. (2010). Water-stable isotopes in the LMDZ4 general circulation model: Model evaluation for present-day and past climates and applications to climatic interpretations of tropical isotopic records. *Journal of Geophysical Research*, *115*, D12118. https://doi.org/10.1029/2009JD013255

Risi, C., Landais, A., Winkler, R., & Vimeux, F. (2013). Can we determine what controls the spatio-temporal distribution of d-excess and ^{17}O-excess in precipitation using the LMDZ general circulation model? *Climate of the Past*, *9*(5), 2173–2193. https://doi.org/10.5194/cp-9-2173-2013

Risi, C., Noone, D., Worden, J., Frankenberg, C., Stiller, G., Kiefer, M., et al. (2012). Process-evaluation of tropospheric humidity simulated by general circulation models using water vapor isotopologues: 1. Comparison between models and observations. *Journal of Geophysical Research*, *117*, D05303. https://doi.org/10.1029/2011JD016621

Risi, C., Ogée, J., Bony, S., Bariac, T., Raz-Yaseef, N., Wingate, L., et al. (2016). The water isotopic version of the Land-Surface Model ORCHIDEE: Implementation, evaluation, sensitivity to hydrological parameters. *Hydrology: Current Research*, *7*(4), 258. https://doi.org/10.4172/2157-7587.1000258

Rozanski, K., Araguás-Araguás, L., & Gonfiantini, R. (1992). Relation between long-term trends of oxygen-18 isotope composition of precipitation and climate. *Science*, *258*(5084), 981–985. https://doi.org/10.1126/science.258.5084.981

Rozanski, K., Araguás-Araguás, L., & Gonfiantini, R. (1993). Isotopic patterns in modern global precipitation. In P. K. Swart, K. C. Lohmann, J. Mckenzie, & S. Savin (Eds.), *Climate change in continental isotopic records* (pp. 1–36). American Geophysical Union.

Salati, E., Dall'Olio, A., Matsui, E., & Gat, J. R. (1979). Recycling of water in the Amazon Basin: An isotopic study. *Water Resources Research*, *15*(5), 1250–1258. https://doi.org/10.1029/WR015i005p01250

Schmidt, G. A., Hoffmann, G., Shindell, D. T., & Hu, Y. (2005). Modeling atmospheric stable water isotopes and the potential for constraining cloud processes and stratosphere-troposphere water exchange. *Journal of Geophysical Research*, *110*, D21314. https://doi.org/10.1029/2005JD005790

Schoenemann, S. W., Steig, E. J., Ding, Q., Markle, B. R., & Schauer, A. J. (2014). Triple water-isotopologue record from WAIS Divide, Antarctica: Controls on glacial-interglacial changes in $^{17}O_{excess}$ of precipitation. *Journal of Geophysical Research: Atmospheres*, *119*, 8741–8763. https://doi.org/10.1002/2014JD021770

Scott, R. L., Knowles, J. F., Nelson, J. A., Gentine, P., Li, X., Barron-Gafford, G., et al. (2021). Water availability impacts on evapotranspiration partitioning. *Agricultural and Forest Meteorology*, *297*, 108251. https://doi.org/10.1016/j.agrformet.2020.108251

Serreze, M. C., Carse, F., Barry, R. G., & Rogers, J. C. (1997). Icelandic Low cyclone activity: Climatological features, linkages with the NAO, and relationships with recent changes in the Northern Hemisphere circulation. *Journal of Climate*, *10*(3), 453–464. https://doi.org/10.1175/1520-0442(1997)010<0453:ilcacf>2.0.co;2

Sha, L., Mahata, S., Duan, P., Luz, B., Zhang, P., Baker, J., et al. (2020). A novel application of triple oxygen isotope ratios of speleothems. *Geochimica et Cosmochimica Acta*, *270*, 360–378. https://doi.org/10.1016/j.gca.2019.12.003

Simmonds, I., & Keay, K. (2002). Surface fluxes of momentum and mechanical energy over the North Pacific and North Atlantic Oceans. *Meteorology and Atmospheric Physics*, *80*(1), 1–18. https://doi.org/10.1007/s007030200009

Steen-Larsen, H. C., Risi, C., Werner, M., Yoshimura, K., & Masson-Delmotte, V. (2017). Evaluating the skills of isotope-enabled general circulation models against in situ atmospheric water vapor isotope observations. *Journal of Geophysical Research: Atmospheres*, *122*, 246–263. https://doi.org/10.1002/2016JD025443

Steen-Larsen, H. C., Sveinbjörnsdottir, A. E., Peters, A. J., Masson-Delmotte, V., Guishard, M. P., Hsiao, G., et al. (2014). Climatic controls on water vapor deuterium excess in the marine boundary layer of the North Atlantic based on 500 days of in situ, continuous measurements. *Atmospheric Chemistry and Physics*, *14*(15), 7741–7756. https://doi.org/10.5194/acp-14-7741-2014

Stenni, B., Masson-Delmotte, V., Johnsen, S., Jouzel, J., Longinelli, A., Monnin, E., et al. (2001). An oceanic cold reversal during the last deglaciation. *Science*, *293*(5537), 2074–2077. https://doi.org/10.1126/science.1059702

Stewart, M. K. (1975). Stable isotope fractionation due to evaporation and isotopic exchange of falling waterdrops: Applications to atmospheric processes and evaporation of lakes. *Journal of Geophysical Research*, *80*(9), 1133–1146. https://doi.org/10.1029/JC080i009p01133

Sutanto, S. J., van den Hurk, B., Dirmeyer, P. A., Seneviratne, S. I., Röckmann, T., Trenberth, K. E., et al. (2014). HESS Opinions "A perspective on isotope versus non-isotope approaches to determine the contribution of transpiration to total evaporation". *Hydrology and Earth System Sciences*, *18*(8), 2815–2827. https://doi.org/10.5194/hess-18-2815-2014

Taupin, J.-D., Coudrain-Ribstein, A., Gallaire, R., Zuppi, G. M., & Filly, A. (2000). Rainfall characteristics ($\delta^{18}O$, $\delta^{2}H$, ΔT and ΔH_t) in western Africa: Regional scale and influence of irrigated areas. *Journal of Geophysical Research*, *105*(D9), 11911–11924. https://doi.org/10.1029/1999JD901032

Tian, L., Yao, T., MacClune, K., White, J. W. C., Schilla, A., Vaughn, B., et al. (2007). Stable isotopic variations in west China: A consideration of moisture sources. *Journal of Geophysical Research*, *112*, D10112. https://doi.org/10.1029/2006JD007718

Tindall, J. C., Valdes, P. J., & Sime, L. C. (2009). Stable water isotopes in HadCM3: Isotopic signature of El Niño-Southern Oscillation and the tropical amount effect. *Journal of Geophysical Research*, *114*, D04111. https://doi.org/10.1029/2008JD010825

Trenberth, K. E., Fasullo, J. T., & Mackaro, J. (2011). Atmospheric moisture transports from ocean to land and global energy flows in reanalyses. *Journal of Climate*, *24*(18), 4907–4924. https://doi.org/10.1175/2011JCLI4171.1

Ueta, A., Sugimoto, A., Iijima, Y., Yabuki, H., & Maximov, T. C. (2014). Contribution of transpiration to the atmospheric moisture in eastern Siberia estimated with isotopic composition of water vapour. *Ecohydrology*, *7*(2), 197–208. https://doi.org/10.1002/eco.1403

Vallet-Coulomb, C., Gasse, F., & Sonzogni, C. (2008). Seasonal evolution of the isotopic composition of atmospheric water vapour above a tropical lake: Deuterium excess and implication for water recycling. *Geochimica et Cosmochimica Acta*, *72*(19), 4661–4674. https://doi.org/10.1016/j.gca.2008.06.025

van der Ent, R. J. (2016). WAM2layersPython version 2.4.08. Retrieved from https://github.com/ruudvdent/WAM2layersPython

van der Ent, R. J., Wang-Erlandsson, L., Keys, P. W., & Savenije, H. H. G. (2014). Contrasting roles of interception and transpiration in the hydrological cycle—Part 2: Moisture recycling. *Earth System Dynamics*, *5*(2), 471–489. https://doi.org/10.5194/esd-5-471-2014

Vimeux, F., Masson, V., Jouzel, J., Stievenard, M., & Petit, J. R. (1999). Glacial-interglacial changes in ocean surface conditions in the Southern Hemisphere. *Nature*, *398*(6726), 410–413. https://doi.org/10.1038/18860

Vuille, M., Bradley, R. S., Werner, M., Healy, R., & Keimig, F. (2003). Modeling $\delta^{18}O$ in precipitation over the tropical Americas: 1. Interannual variability and climatic controls. *Journal of Geophysical Research*, *108*(D6), 4174. https://doi.org/10.1029/2001JD002038

Wang, L., Good, S. P., & Caylor, K. K. (2014). Global synthesis of vegetation control on evapotranspiration partitioning. *Geophysical Research Letters*, *41*, 6753–6757. https://doi.org/10.1002/2014GL061439

Wang, S., Lei, S., Zhang, M., Hughes, C., Crawford, J., Liu, Z., & Qu, D. (2022). Spatial and seasonal isotope variability in precipitation across China: Monthly isoscapes based on regionalized fuzzy clustering. *Journal of Climate*, *35*(11), 3411–3425. https://doi.org/10.1175/JCLI-D-21-0451.1

Wang, S., Zhang, M., Che, Y., Chen, F., & Qiang, F. (2016a). Contribution of recycled moisture to precipitation in oases of arid central Asia: A stable isotope approach. *Water Resources Research*, *52*, 3246–3257. https://doi.org/10.1002/2015WR018135

Wang, S., Zhang, M., Che, Y., Zhu, X., & Liu, X. (2016b). Influence of below-cloud evaporation on deuterium excess in precipitation of arid central Asia and its meteorological controls. *Journal of Hydrometeorology*, *17*(7), 1973–1984. https://doi.org/10.1175/JHM-D-15-0203.1

Wang-Erlandsson, L., Bastiaanssen, W. G. M., Gao, H., Jägermeyr, J., Senay, G. B., van Dijk, A. I. J. M., et al. (2016). Global root zone storage capacity from satellite-based evaporation. *Hydrology and Earth System Sciences*, *20*(4), 1459–1481. https://doi.org/10.5194/hess-20-1459-2016

Wei, Z., & Lee, X. (2019). The utility of near-surface water vapor deuterium excess as an indicator of atmospheric moisture source. *Journal of Hydrology*, *577*, 123923. https://doi.org/10.1016/j.jhydrol.2019.123923

Wei, Z., Lee, X., Liu, Z., Seeboonruang, U., Koike, M., & Yoshimura, K. (2018). Influences of large-scale convection and moisture source on monthly precipitation isotope ratios observed in Thailand, Southeast Asia. *Earth and Planetary Science Letters*, *488*, 181–192. https://doi.org/10.1016/j.epsl.2018.02.015

Wei, Z., Yoshimura, K., Wang, L., Miralles, D. G., Jasechko, S., & Lee, X. (2017). Revisiting the contribution of transpiration to global terrestrial evapotranspiration. *Geophysical Research Letters*, *44*, 2792–2801. https://doi.org/10.1002/2016GL072235

Welker, J. M. (2000). Isotopic ($\delta^{18}O$) characteristics of weekly precipitation collected across the USA: An initial analysis with application to water source studies. *Hydrological Processes*, *14*(8), 1449–1464. https://doi.org/10.1002/1099-1085(20000615)14:8<1449::aid-hyp993>3.0.co;2-7

Welker, J. M. (2012). ENSO effects on $\delta^{18}O$, $\delta^{2}H$ and d-excess values in precipitation across the U.S. using a high-density, long-term network (USNIP). *Rapid Communications in Mass Spectrometry*, *26*(17), 1893–1898. https://doi.org/10.1002/rcm.6298

Welp, L. R., Randerson, J. T., Finlay, J. C., Davydov, S. P., Zimova, G. M., Davydova, A. I., & Zimov, S. A. (2005). A high-resolution time series of oxygen isotopes from the Kolyma River: Implications for the seasonal dynamics of discharge and basin-scale water use. *Geophysical Research Letters*, *32*, L14401. https://doi.org/10.1029/2005GL022857

Werner, M., Langebroek, P. M., Carlsen, T., Herold, M., & Lohmann, G. (2011). Stable water isotopes in the ECHAM5 general circulation model: Toward high-resolution isotope modeling on a global scale. *Journal of Geophysical Research*, *116*, D15109. https://doi.org/10.1029/2011JD015681

Winnick, M. J., Chamberlain, C. P., Caves, J. K., & Welker, J. M. (2014). Quantifying the isotopic 'continental effect'. *Earth and Planetary Science Letters*, *406*, 123–133. https://doi.org/10.1016/j.epsl.2014.09.005

Wong, T. E., Nusbaumer, J., & Noone, D. C. (2017). Evaluation of modeled land-atmosphere exchanges with a comprehensive water isotope fractionation scheme in version 4 of the Community Land Model. *Journal of Advances in Modeling Earth Systems*, *9*(2), 978–1001. https://doi.org/10.1002/2016MS000842

Worden, J., Noone, D., Bowman, K., Beer, R., Eldering, A., Fisher, B., et al. (2007). Importance of rain evaporation and continental convection in the tropical water cycle. *Nature*, *445*(7127), 528–532. https://doi.org/10.1038/nature05508

Xia, Z., & Winnick, M. J. (2021). The competing effects of terrestrial evapotranspiration and raindrop re-evaporation on the deuterium excess of continental precipitation. *Earth and Planetary Science Letters*, *572*, 117120. https://doi.org/10.1016/j.epsl.2021.117120

Yoshimura, K., Kanamitsu, M., Noone, D., & Oki, T. (2008). Historical isotope simulation using reanalysis atmospheric data. *Journal of Geophysical Research*, *113*, D19108. https://doi.org/10.1029/2008JD010074

Zhou, S., Yu, B., Zhang, Y., Huang, Y., & Wang, G. (2018). Water use efficiency and evapotranspiration partitioning for three typical ecosystems in the Heihe River Basin, northwestern China. *Agricultural and Forest Meteorology*, *253–254*, 261–273. https://doi.org/10.1016/j.agrformet.2018.02.002